“CORTICAL DELTA” IN THE MEDULLA OF SLEEPING INFANT RATS

Midha Ahmad[1], Jangjin Kim[2], Brett Dwyer[1], Greta Sokoloff[1,3], and Mark S. Blumberg[1,3*]

[1]Department of Psychological & Brain Sciences, University of Iowa, Iowa City, IA 52242, USA
[2]Department of Psychology, Kyungpook National University, Daegu, 41566, Republic of Korea
[3]Iowa Neuroscience Institute, University of Iowa, Iowa City, IA 52242 USA

*Lead contact

Corresponding Author: Mark Blumberg (mark-blumberg@uiowa.edu)

SUMMARY

In early development when sleep is the most prevalent behavioral state, active (REM) sleep is preeminent before it is supplanted by quiet (non-REM) sleep. In rats, the developmental increase in quiet sleep is accompanied by the sudden emergence of the cortical delta rhythm (0.5-4 Hz) around postnatal day (P) 12. We sought to explain the emergence of cortical delta by assessing developmental changes in the activity of the parafacial zone (PZ), a medullary structure thought to regulate quiet sleep in adults. We recorded from PZ and predicted an age-related increase in neural activity during increasing periods of delta-rich cortical activity. Instead, we discovered a state-dependent pattern of neural activity comprising rhythmic bursts—separated by periods of complete silence—that are phase-locked to a local delta rhythm. Moreover, PZ and cortical delta were coherent at P12, but not at P10. PZ delta was also phase-locked to respiration, suggesting that reported links between respiration and cortical delta are traceable to sleep-dependent modulation of PZ activity by respiratory pacemakers in the ventral medulla. Disconnecting the main olfactory bulbs from the cortex did not diminish cortical delta, indicating that the influence of respiration on delta at this age is not mediated indirectly through nasal breathing. Finally, we observed increasing expression of parvalbumin-expressing terminals in PZ across these ages, supporting a role for GABAergic inhibition in PZ's rhythmicity. The discovery of delta-rhythmic neural activity in the medulla—at the moment of cortical delta's developmental emergence—opens a new path to understanding the brainstem's role in regulating quiet sleep.

INTRODUCTION

The brain and body are rich with rhythms.[1–4] Some rhythms have transparently obvious functions, such as the breathing movements that exchange oxygen and carbon dioxide in the lungs. But the functions of numerous other rhythms, especially brain rhythms, are less obvious. Among these are rhythms that occur during sleep, including the cortical delta rhythm (0.5-4 Hz) that characterizes quiet sleep (QS; or non-REM sleep).[5,6] Cortical delta is a key player in many aspects of adult sleep. For example, because its amplitude registers the intensity of QS, cortical delta is central to the notion of sleep homeostasis.[7] Functionally, cortical delta coordinates with other forebrain rhythms to promote learning and neural plasticity.[5,6,8–10] However, these features of adult sleep are absent in early infancy because cortical delta develops relatively late: In rats, it does not emerge until around postnatal day (P) 12,[11,12] at which time QS is just beginning to supersede active sleep (AS; or REM sleep) as the predominant sleep state.[11–14]

For many decades, sleep researchers debated whether the brainstem contains a system for regulating QS that complements the system in the forebrain.[15,16] Recently, evidence for brainstem involvement was strengthened by the discovery in adult mice that the parafacial zone (PZ), an area located immediately dorsal to the facial nerve in the medulla, regulates QS.[17,18] In addition, unit recordings from the PZ of adult rats identified a diversity of state-dependent neurons, including neurons that fire preferentially during QS.[19] According to one model,[20] when GABAergic PZ neurons are activated during QS, they inhibit glutamatergic neurons in the parabrachial nucleus that project to the basal forebrain (BF), resulting in decreased cortical arousal and increased cortical delta.

We hypothesized that cortical delta emerges in part due to developmental changes in PZ and related brainstem circuits that regulate QS. Here, we test this hypothesis by recording PZ and cortical activity in P10 and P12 rats across the sleep-wake cycle. We predicted that developmental changes in the <u>rate</u> of PZ firing would track the onset of cortical delta. Instead, we discovered a striking <u>pattern</u> of PZ activity comprising population-level rhythmic bursts during QS. Even more surprising, the rhythmic bursts were phase-locked to a local delta rhythm that, in turn, was coherent with cortical delta. The rhythmic bursts

were also phase-locked with the regular respiration that characterizes QS.[21,22] These findings introduce an unexpected dimension to the brainstem's role in sleep regulation and function, raise novel questions about the mechanisms enabling the expression of long-range communication in the infant brain, and open a new path to understanding the intimate connection between a sleep-dependent brain rhythm and the most bodily of rhythms—respiration.[23–26]

RESULTS

We recorded activity in PZ and frontal cortex using linear silicon electrodes in unanesthetized, head-fixed P10 and P12 rats as they cycled freely between sleep and wake (**Figure 1A-B;** N = 8 pups/age; P10: 150 units; P12: 136 units; 12-30 units/pup). Analyses were performed only when histology confirmed electrode placements in PZ, as identified previously (**Figure 1C**).[20] Behavioral states were classified based on respiration, limb movements, and cortical and/or PZ activity (**Figure 1D**; see Methods).

PZ units exhibit rhythmic bursts during QS at P12

For each PZ unit at P12, we calculated its mean firing rate within each state (**Figure 1E**). Firing rates for each state were then averaged within pups (**Figure 1F**). ANOVA revealed a significant effect of behavioral state ($F_{(1.29,9.06)} = 26.15$, $p < .001$, adj. $\eta p^2 = 0.76$), with unexpectedly higher PZ firing rates during AS than during QS or wake. However, closer inspection of population-level PZ unit activity revealed a pattern of rhythmic bursting during QS (**Figure 2A**). These rhythmic bursts occurred only during periods of cortical delta and regular breathing. Moreover, PZ's rhythmicity did not result merely from relative increases and decreases in spiking activity; instead, we observed PZ bursts with intervening periods of total silence lasting approximately 0.1 to 0.5 s (**Figure 2B**). ANOVA revealed a significant effect of behavioral state on the duration of these silent periods, ($F_{(2,14)} = 44.18$, $p < .001$, adj. $\eta p^2 = 0.84$), with significantly longer periods occurring during QS than during AS or wake (**Figure 2C**).

A local delta rhythm in PZ during QS at P12

The rhythmic bursting of PZ units during QS appeared to be timed to the troughs of cortical delta and, surprisingly, to the troughs of a similar delta rhythm in PZ (hereafter, PZ delta). To determine whether PZ and cortical delta have similar properties, we generated mean power spectra in the two structures (normalized within each structure; **Figure 3A, top**) and quantified mean delta power (**Figure 3A, bottom**). Mean delta power was significantly greater during QS than AS in both PZ and cortex (PZ: $t_{(7)} = 3.65$, $p < .01$, Hedge's $g = 1.12$; cortex: $t_{(6)} = 9.26$, $p < .001$, Hedge's $g = 2.95$).

The QS-related increase in delta power in PZ and cortex was accompanied by peak coherence at delta frequencies (**Figure 3B**); no such coherence peak was found during AS. Mean delta coherence was significantly greater during QS than AS ($t_{(5)} = 5.22$, $p < .01$, Hedge's $g = 1.70$; **Figure 3C**). A coherence peak was also found during AS, but at 5 Hz, which is within the range of theta (4-8 Hz) at this age (**Figure 3B**).[27] However, PZ units were not phase-locked with theta (data not shown), suggesting that theta is not generated locally within PZ, but is rather volume-conducted from a nearby region.

To assess whether PZ delta is produced locally, we computed the distribution of each PZ unit's activity in relation to the phase of PZ delta. The distributions were averaged within pups before further analysis. During QS, PZ units exhibited a strong tendency to fire near the trough of PZ delta (**Figure 4A, top**). This tendency was not spurious, as no such relation was found during AS (**Figure 4A, bottom**). Phase-locking values (PLVs) of unit activity to PZ delta were computed, z-transformed, and assessed using a conservative significance criterion ($z = 3.29$, $p < .001$). During QS, 100% (8/8) of the pups exhibited significant PLVs; during AS, only 25% (2/8) of pups exceeded this threshold. We also computed circular concentration coefficients (kappa) of the von Mises distribution (**Figure 4C**); this coefficient reflects the dispersion of the distribution, with higher values indicating tight clustering around specific phases.[28] Mean kappa values were significantly greater during QS than AS ($t_{(7)} = 7.42$, $p < .001$, Hedge's $g = 2.28$). The strong phase-locking of PZ units to PZ delta indicates that the rhythm is produced locally.

QS-related activity in PZ and cortex is weaker at P10

We also performed recordings at P10, an age when cortical delta is just beginning to emerge and before QS durations begin to increase.[11–14] Similar to P12, firing rates at P10 were significantly state dependent ($F_{(2,14)}$ = 14.253, p < .001, adj. ηp^2 = 0.62); firing rate was again highest during AS, though only significantly higher in relation to wake (**Figure S1**). PZ bursting during QS was evident at P10, but it was not as rhythmic as at P12 (**Figure 5A**). Also, as expected given the nascent nature of QS and delta at P10, bouts of PZ bursting were relatively fragmented. Also, PZ bursts were again separated by periods of PZ silence, but these periods appeared less stable at this age (**Figure 5B**). Nonetheless, periods of PZ silence were state dependent ($F_{(2,14)}$ = 25.12, p < .001, adj. ηp^2 = 0.78), with a significantly higher proportion of silent periods occurring during QS than during AS or wake (**Figure 5C**).

We next compared raw delta power at P10 and P12 (**Figure S2**). Cortical delta power was relatively low at both ages but increased between P10 and P12. In contrast, PZ delta power was relatively pronounced at P10, and even more so at P12. Thus, at these early ages, PZ may provide a more sensitive indicator of QS-related delta than cortex.

Further support for this notion comes from the assessment of normalized power spectra at P10 (**Figure 6A**): Mean delta power was significantly greater during QS than AS in PZ ($t_{(7)}$ = 2.94, p < .05, Hedge's g = 0.90), but not in cortex ($t_{(7)}$ = 1.97, Hedge's g = 0.60). Also, there was only a meager peak in coherence at delta frequencies (**Figure 6B**). Most important, however, was that mean delta coherence was not significantly different between QS and AS at this age ($t_{(7)}$ = 0.145, Hedge's g = 0.04; **Figure 6C**). Finally, PZ units were significantly phase-locked to PZ delta at this age, even though delta occurred in relatively brief bouts (kappa: $t_{(7)}$ =2.78, p < .05, Hedge's g = 0.86; **Figure S3**).

PZ activity is modulated by respiration

Respiratory regularity and irregularity are characteristic of QS and AS, respectively, in infant rats.[21] We confirmed this same relationship in our P12 rats: mean inter-breath interval was significantly longer ($t_{(7)}$ = 5.50, p < .001, Hedge's g = 1.69) and variance was

significantly smaller ($t_{(7)}$ = 12.31, p < .001, Hedge's g = 3.79) during QS than AS (**Figure 7A**). Moreover, during QS, respiratory power showed a peak at ~2 Hz, similar to PZ and cortical delta. During AS, peak respiratory power also peaked within delta frequencies, but the peak was broader and more variable than that during AS, consistent with the irregularity of breathing during this sleep state (**Figure 7B**).

We next assessed the association between QS-related respiration and PZ population firing rate (**Figure 7C-D**). There were clear and significant peaks in firing rate that occurred after the onset of inspiration (Z = 44.43, p < .001). This result was obtained using a conservative threshold for defining PZ peak firing rates; similar results were also obtained using more liberal thresholds (**Figure S4**).

Disconnecting the olfactory bulbs at P12 does not diminish the expression of cortical delta

Respiratory modulation of cortical delta could be mediated directly via ascending projections from PZ or indirectly via the influence of nasal breathing on LFPs in the olfactory bulb (**Figure S5**).[25] We tested the latter mechanism at P12 by comparing cortical LFPs in a small cohort of pups (n = 4/group) with and without bilateral transection of the lateral olfactory tract (**Figure S6**). First, the mean power spectrum for the shams closely resembled that found in a separate group of pups (see **Figure S2**). Second, delta power during QS was not diminished by transection at this age; if anything, mean cortical power was higher in this group. Finally, the 2-Hz peak was considerably sharper in the transected pups than in the shams. These findings not only rule out a major role for an indirect influence of nasal breathing and olfactory-bulb oscillations on cortical delta at this age, but they also raise the possibility that the indirect influence interferes with the expression of cortical delta. These findings are also consistent with a previous study that reported small effects of similar olfactory manipulations on cortical delta in adult mice.[25]

PZ-related expression of parvalbumin increases between P8 and P12

Expression of the calcium-binding protein, parvalbumin (PV), is a marker of inhibitory interneurons.[29,30] Given the general importance of inhibition for brain rhythms[29,30] and,

more specifically, the role of PV in shaping rhythmic brain activity in nearby structures,[31] we compared PV expression in PZ in P8, P10, and P12 rats (n = 3-4 pups/age; **Figure S7**). Whereas PV expression was sparse at P8, we observed increasingly dense labeling of PV terminals at P10 and P12.

DISCUSSION

We report in infant rats an unexpected finding of QS-dependent rhythmic bursting in PZ, a medullary structure that is implicated in the regulation of QS in adults.[20,32] The rhythmic bursting in PZ is phase-locked to the troughs of a local delta rhythm that, in turn, is coherent with cortical delta. PZ and cortical delta emerge together and become coherent between P10 and P12, suggesting a mechanistic link between the two rhythms. Finally, PZ activity during QS is phase-locked to the regular respiratory rhythm that characterizes that sleep state. Altogether, these findings open the door to a new mechanistic understanding of the brainstem's contributions to the regulation of sleep, sleep-related rhythms, and the expression of long-range functional connectivity in early development.

Our findings also inform the decades-long debate about the contributions of the brainstem to cortical rhythmicity.[15] The delta rhythm is a reliable and prominent feature of forebrain activity during QS,[33] and this rhythm can be observed in the cortex even after it is surgically disconnected from the brainstem.[16,34] However, early transection studies also implicated the caudal brainstem in the synchronization of cortical rhythms.[35–37] The current findings go much further than those earlier studies to demonstrate in a medullary structure the presence of rhythmic bursts of neural activity that are phase-locked to a local delta rhythm. Our findings also suggest that the delta-producing system in PZ is mechanistically and functionally associated with the respiratory pacemaker in the ventral medulla.[38] Thus, we can situate this delta-production system within the broader network of rhythm-generating circuitry in the brainstem, thereby revealing new possibilities for understanding the links among neural oscillations, respiration, and sleep.

Interpreting PZ's contributions to sleep and delta

Beginning a decade ago, PZ's role in the regulation of QS was identified and characterized in adult mice.[17,18] According to the model developed from this work, GABAergic neurons in PZ increase their activity during QS and thus inhibit downstream neurons in the parabrachial nucleus (PB); the result is decreased excitatory drive to the arousal-producing basal forebrain (BF), thereby enabling the expression of QS and cortical delta. A subsequent study using adult rats identified PZ neurons with diverse state-dependent profiles, including a plurality (40%) that were selectively active during QS;[19] however, population-level PZ activity and LFP were not reported, an important difference from the current study that perhaps explains the detection here of rhythmic bursting and delta in PZ. Because the current study also differs in its focus on a developmental period when cortical delta is first emerging, future studies of population activity in PZ are necessary to characterize changes in activity patterns beyond 12 days of age.

The discovery of rhythmic bursts in PZ that are phase-locked with local delta complicates the current model of PZ function described above. Instead, the current findings raise the possibility that PZ entrains cortical delta, perhaps via PZ's direct connections with such structures as PB, BF, anterior hypothalamus, or thalamus (**Figure S5**).[56] Alternatively, there may be no direct causal link between PZ and cortical delta; one way to test for such a link is to optogenetically perturb PZ's rhythmic bursting during QS and assess its immediate effect on cortical delta. Failure to find an effect would raise different questions about the functional significance of PZ delta and its co-emergence with cortical delta at the end of the second postnatal week.

The role of inhibition in PZ's rhythmic spiking activity

It should not be overlooked that PZ activity at P12 was highest during AS, not QS. Thus, the key finding here relates not to the <u>rate</u> of PZ's neural activity, but its <u>patterning</u>. The rhythmic bursts during QS are perhaps the most salient feature of PZ activity at this age. However, the interburst periods when spiking was completely absent—not merely

reduced—are significant, as they suggest the influence of powerful rhythmic inhibition. In other words, it is possible that PZ activity at P12 would be similar during AS and QS, but for those periods of complete silence that are “carved out” of ongoing neural activity during QS. Such a mechanism could inadvertently yield increased firing rates during AS, a possibility that encourages caution when interpreting state-dependent differences in firing rates without considering state-dependent differences in firing patterns.

The onset of delta at P12 may be related to at least two major changes in inhibitory processing that happen around that age. First, there is the proliferation of PV-expressing inhibitory neurons; our finding of increased proliferation between P8 and P12 is consistent with previous findings in the auditory brainstem, in which PV-labelled cells emerge between P8 and P12.[39] In frontal cortex, PV-labelled cells first appear at P11 and are adult-like by P21,[40] mirroring the development of cortical delta power.[12] Second, there is the transition in GABA’s effects on postsynaptic cells from depolarizing to hyperpolarizing (“GABA switch”),[41–43] mediated by increased expression of the K^+–Cl^- cotransporter-2 (KCC2). In the forebrain, the GABA switch occurs in rats between P5 and P15.[44,45] The developmental relations between GABA’s changing postsynaptic effects and the expression of delta are not yet established, but recent evidence in adult mice suggests that GABA’s postsynaptic inhibitory effects are dynamically regulated across sleep and wake to influence the expression of cortical delta.[46]

The P8-to-P12 developmental window also includes other major changes in brain and behavior, such as the transition from discontinuous to continuous cortical activity,[47–49] the emergence of hippocampal theta,[27] the proliferation and diversification of inhibitory interneurons,[40,50–52] an acceleration in the deposition of myelin,[53] the onset of true whisking[54], and the locomotor transition from punting to crawling.[55] Accordingly, the developmental emergence of rhythmic bursting and delta in PZ should be viewed within this broader context of a period of transformational change and, consequently, a heightened sensitivity to developmental disruption.

The source of inhibitory input that enables rhythmic bursting in PZ is not yet clear. One study in adult mice identified strong GABAergic inputs to PZ from the intermediate

246 reticular nucleus (IRt), the deep mesencephalic nucleus (DpMe), the pontine reticular
247 nucleus (PnO), and the lateral hypothalamus (LH).[56] The last three are notable for their
248 roles in infant[57,58] and/or adult[59] sleep regulation, and thus may contribute to the sleep-
249 dependent modulation of PZ.

250 But it is IRt,[4,31,60] a structure that is adjacent to PZ and provides it with some of its
251 strongest GABAergic input,[56] that may be particularly relevant for understanding PZ's
252 rhythmic behavior: In adult mice, the production of rhythmic vibrissal movements (i.e.,
253 whisking) has been traced to premotor neurons within a "vibrissal zone" in IRt that, under
254 the resetting influence of the respiratory pacemaker in the ventral medulla, enables
255 phase-locking of whisking and sniffing.[60] Importantly, these premotor IRt neurons depend
256 on a local circuit comprising PV interneurons for the transition from tonic to bursting
257 modes.[31] We suggest that the PZ system that enables rhythmic bursting during QS is part
258 of the larger oscillatory network that includes IRt and that integrates a diversity of rhythmic
259 behaviors and neural oscillations.[60,61] Moreover, because PZ also receives prominent
260 state-related input, it is well positioned to integrate sleep-related and respiratory input to
261 produce a rhythm such as delta.

262 **Respiration modulates (sub)cortical delta**

263 The notion that PZ is part of a larger oscillatory network in IRt is further supported by
264 respiration's modulatory role.[4] Evidence for such a role can be traced to the ventral
265 respiratory group, a collection of medullary structures that includes the preBötzinger
266 complex (preBötC), the pacemaker of inspiration.[38] There exist a diversity of efferent
267 projections from preBötC to brainstem, hypothalamic, and thalamic structures,[62] including
268 a direct projection to the area in IRt discussed above that governs the phase-locking of
269 whisking and sniffing.[60] As there is no known direct projection from preBötC to PZ,
270 another structure—perhaps IRt—may mediate the respiratory modulation of PZ activity
271 observed here.

272 Considerable effort has been devoted in the past decade to understanding when and how
273 respiration influences the expression of cortical slow waves, including delta, and the

274 functional implications of that influence across sleep-wake states.[23–25,63–65] Of particular
275 relevance to the present study, Karalis and Sirota recently posited the existence in adult
276 mice of a brainstem structure that conveys respiration-related input directly to frontal
277 cortex (**Figure S5**).[25] They also considered whether respiration entrains cortical delta
278 indirectly via the effects of nasal breathing on olfactory-bulb rhythmicity and, in turn,
279 cortical rhythmicity. Because experimental manipulation of activity in the olfactory bulbs
280 reduced but did not prevent respiratory entrainment of cortical delta, it was concluded that
281 entrainment results primarily from an ascending signal from preBötC that they referred to
282 as a respiratory corollary discharge (RCD); indeed, preBötC has few direct projections to
283 the forebrain, but one of its strongest is to mediodorsal thalamus,[62] which has strong
284 functional ties with frontal cortex.[66] Similarly, we found here in P12 rats that disconnecting
285 the main olfactory bulbs has no discernible effect on cortical delta, thus suggesting that a
286 direct respiratory influence from the brainstem is most prominent at this age. That
287 influence could arise directly from PZ or from a third structure that projects independently
288 to PZ and cortex.

289 **Conclusions and Future Directions**

290 Chemogenetic and optogenetic manipulations in adult mice suggest that PZ and nearby
291 structures contribute to the regulation of QS, including delta.[20,67] At this time, however,
292 we do not know how those manipulations influence rhythmic bursting within PZ and the
293 temporal expression of cortical delta. To assess PZ's functional significance, such data
294 are needed in both infant and adult animals. Future studies should also assess similarities
295 and differences in how PZ and cortical delta develop beyond P12, including their
296 homeostatic responses to sleep deprivation.[68]

297 Whereas fast brain rhythms (e.g., sleep spindles, gamma) typically reflect local neural
298 processes, slower rhythms are suitable to long-distance communication.[2,29,30] That delta
299 is expressed coherently between medulla and cortex at P12 is consistent with this general
300 principle governing long-distance communication in the brain. Moreover, the current
301 finding of contemporaneous emergence of delta in PZ and cortex around P12 parallels a
302 similar finding at this age of parallel emergence of a coherent theta rhythm (4-8 Hz) in

hippocampus and red nucleus.[27] Thus, we now have two examples of slow rhythms that exhibit coordinated activity across forebrain and brainstem, and that emerge during the same brief developmental window. The hierarchical nesting of faster rhythms within slower ones may mirror a similarly hierarchical developmental process, with potential implications for the emergence of behavior and cognition in typically and atypically developing animals.[2,30]

Acknowledgments
This research was supported by a grant from the National Institutes Health (R37-HD081168 to M.S.B.)

Author Contributions
Conceptualization, M.A., G.S., and M.S.B.; Methodology, M.A., J.K, B.D., G.S., and M.S.B.; Software: M.A. and J.K.; Formal Analysis: M.A. and J.K.; Investigation: M.A. and B.D.; Data Curation: M.A.; Writing – Original Draft, M.A. and M.S.B.; Writing – Review & Editing, M.A., G.S., and M.S.B.; Visualization: M.A., J.K., B.D., G.S., and M.S.B.; Funding Acquisition, G.S. and M.S.B.; Resources, G.S. and M.S.B.; Supervision, G.S. and M.S.B.

Declaration of Interests
The authors declare no competing interests.

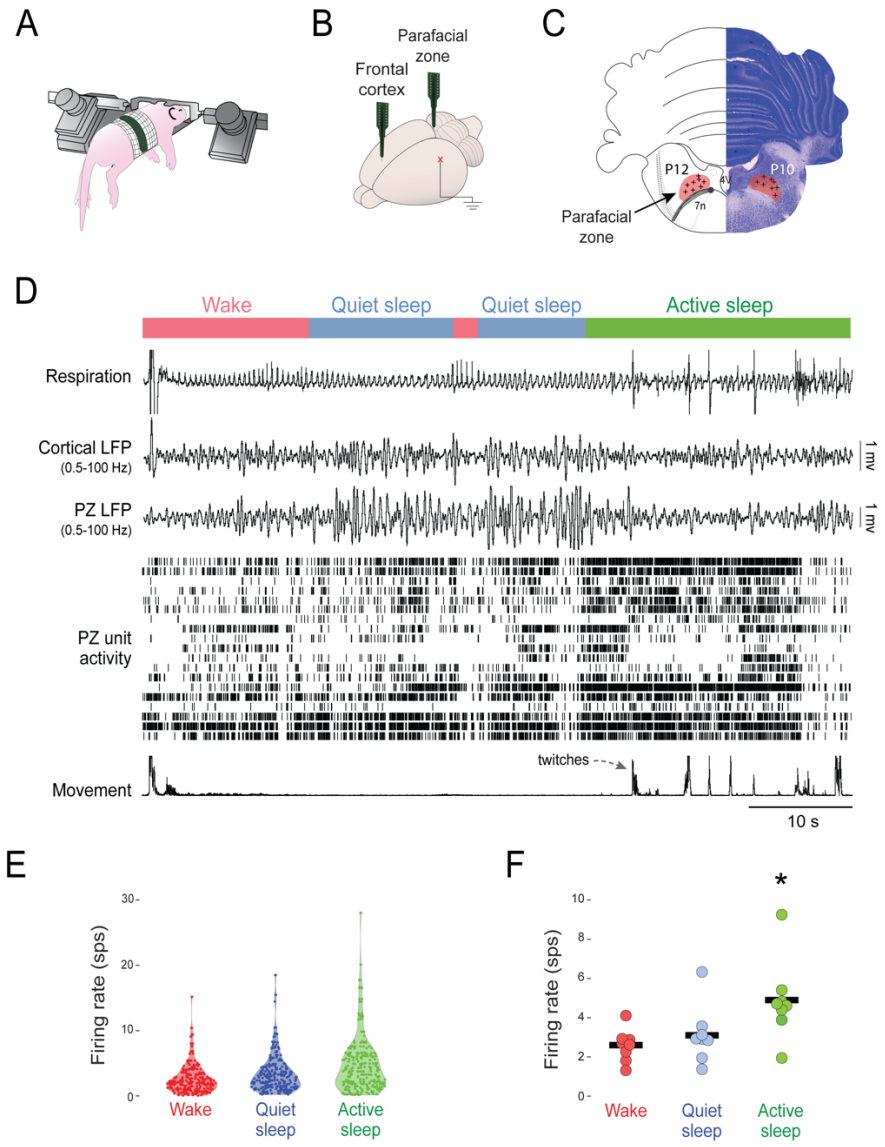

Figure 1. Neural activity in the parafacial zone (PZ) and frontal cortex of infant rats across sleep-wake states

(A) Neural activity and behavior were recorded in head-fixed pups.

(B) Silicon electrodes were inserted into PZ and ipsilateral frontal cortex. A ground/reference electrode was inserted into lateral parietal cortex in the contralateral hemisphere.

(C) Electrode locations within PZ were confirmed histologically in pups at P12 and P10 (n = 8/age).

(D) Representative recording from a P12 rat cycling between wake (red), quiet sleep (blue), and active sleep (green); this color scheme is used for all figures. From top: respiration (inspiration up), cortical and PZ LFP, PZ unit activity, and limb movement.

(E) Violin plots showing mean firing rates (spikes/s) for all recorded PZ units (n = 136) during wake, quiet sleep, and active sleep in P12 rats.

(F) Mean firing rate (spikes/s) of PZ units for P12 rats during wake, quiet sleep, and active sleep. Individual data points are average values for pups. Asterisk denotes significant difference from other two groups.

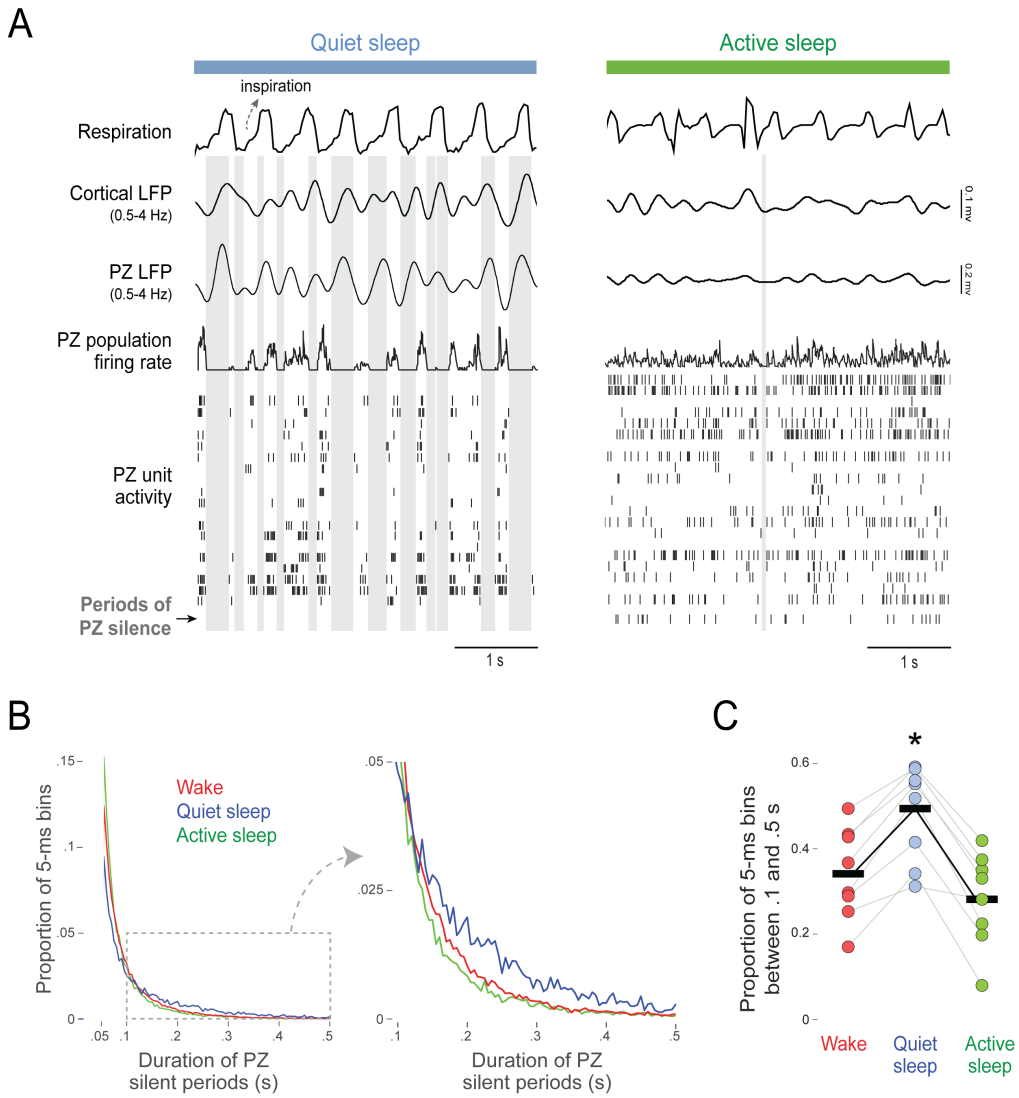

Figure 2. PZ units exhibit rhythmic bursting during quiet sleep in P12 rats
(A) Representative 4-s recordings during quiet sleep (left) and active sleep (right). From top: respiration, cortical and PZ LFP, PZ population firing rate (i.e., the mean firing rate across all PZ single units), and PZ unit activity. Gray vertical bars indicate periods in which all PZ units were silent for at least 50 ms.
(B) Left: Probability distribution of the duration of PZ silent periods (5-ms bins beginning at 0.05 s) during wake (red), quiet sleep (blue), and active sleep (green). Data are pooled across 8 pups. Total number (range) of silent periods: Wake: 54,984 (3,597-9,907); QS: 38,039 (485-17,746); AS: 34,822 (704-10,951). Right: The area within the dotted gray box at left is expanded to show the higher proportion of silent periods with durations between .1 and .5 s during quiet sleep.
(C) Mean proportion of 5-ms bins in which PZ population activity was silent for durations of .1 to .5 s during wake, quiet sleep, and active sleep. Individual data points are average values for pups. Gray lines connect data from the same individual pups. Asterisk denotes significant difference from other two groups.

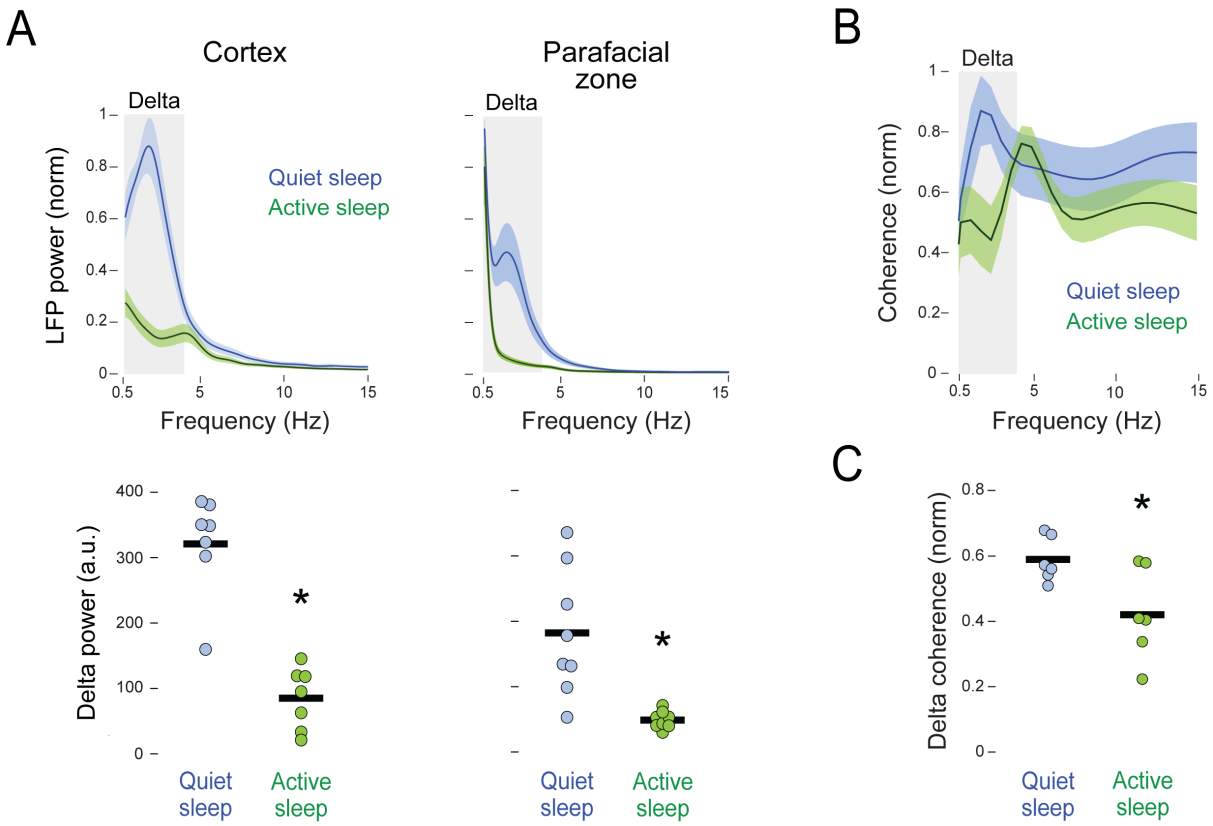

Figure 3. Delta rhythms in PZ and frontal cortex are coherent in P12 rats
(A) Top: Mean (± SEM) LFP power spectra for frontal cortex (left) and PZ (right) during quiet and active sleep. Gray zones indicate delta frequencies (0.5-4 Hz). Bottom: Mean power (arbitrary units, a.u.) within delta frequencies during quiet and active sleep. Data points show power for individual pups. Asterisks denote significant difference between the two groups.
(B) Mean (± SEM) LFP coherence between frontal cortex and PZ during quiet and active sleep. Gray zone indicates delta frequencies (0.5-4 Hz).
(C) Mean normalized (norm) delta coherence for each pup during quiet and active sleep. Coherence values were normalized across both sleep states. Individual data points are average values for pups. Asterisk denotes significant difference between the two groups.

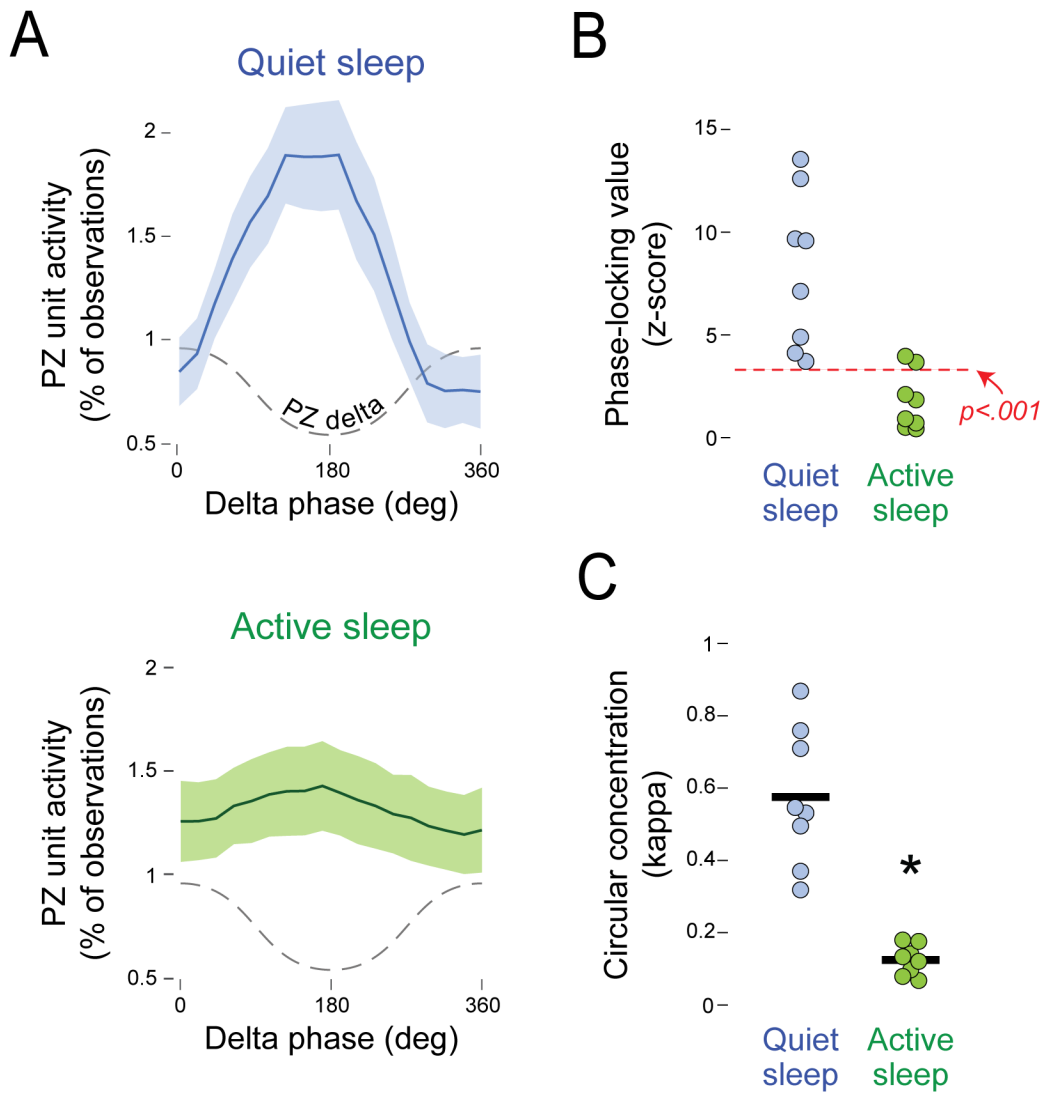

Figure 4. PZ units are phase-locked with local delta during quiet sleep in P12 rats
(A) Mean (± SEM) PZ unit activity in relation to delta phase in PZ during quiet sleep (top) and active sleep (bottom). Delta phase is illustrated with dashed lines.
(B) Phase-locking values (z-scored) of PZ units in relation to local delta phase during quiet and active sleep. Individual data points are average values for pups. Red dotted line indicates a significance level of $p < .001$ based on a z-score of 3.29.
(C) Mean circular concentration coefficients (kappa) of PZ unit activity in relation to local delta phase during quiet and active sleep. Individual data points are average values for pups. Asterisk denotes significant difference between the two groups.

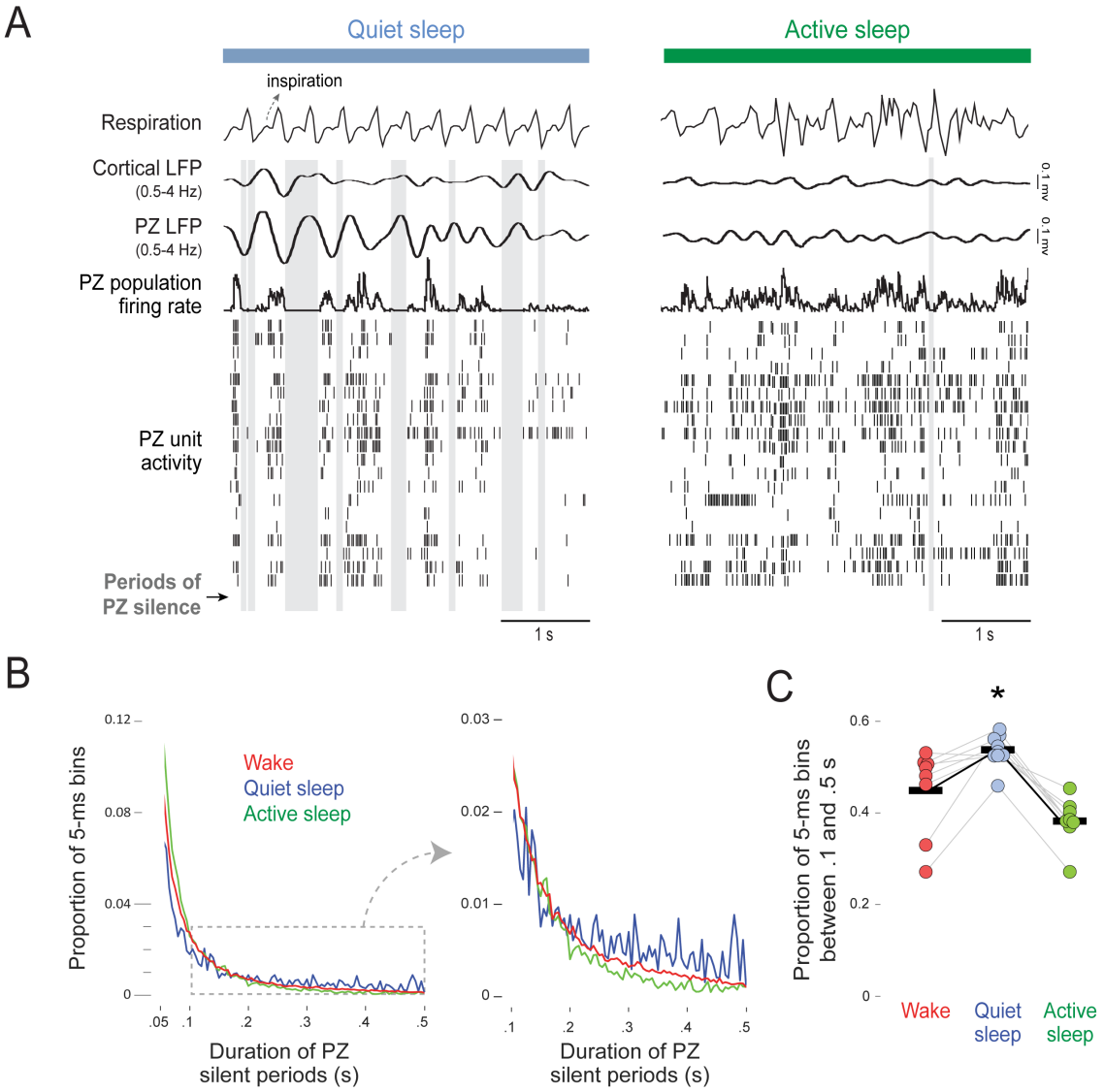

Figure 5. Bursting of PZ units is less regular in P10 rats

(A) Representative 4-s recordings during quiet sleep (left) and active sleep (right). From top: respiration, cortical and PZ LFP, PZ population firing rate (i.e., the mean firing rate across all PZ single units), and PZ unit activity. Gray vertical bars indicate periods in which all PZ units were silent for at least 50 ms.

(B) Left: Probability distribution of the duration of PZ silent periods (5-ms bins beginning at 0.05 s) during wake (red), quiet sleep (blue), and active sleep (green). Data are pooled across 8 pups. Total number (range) of silent periods: Wake: 40.308 (3593-7097); QS: 9,320 (40-2988); AS: 12,361 (200-2877). Right: The area within the dotted gray box at left is expanded to show the higher proportion of silent periods with durations between .1 and .5 s during quiet sleep.

(C) Mean proportion of 5-ms bins in which PZ population activity was silent for durations of .1 to .5 s during wake, quiet sleep, and active sleep. Individual data points are average values for pups. Gray lines connect data from the same individual pups. Asterisk denotes significant difference from the other two groups.

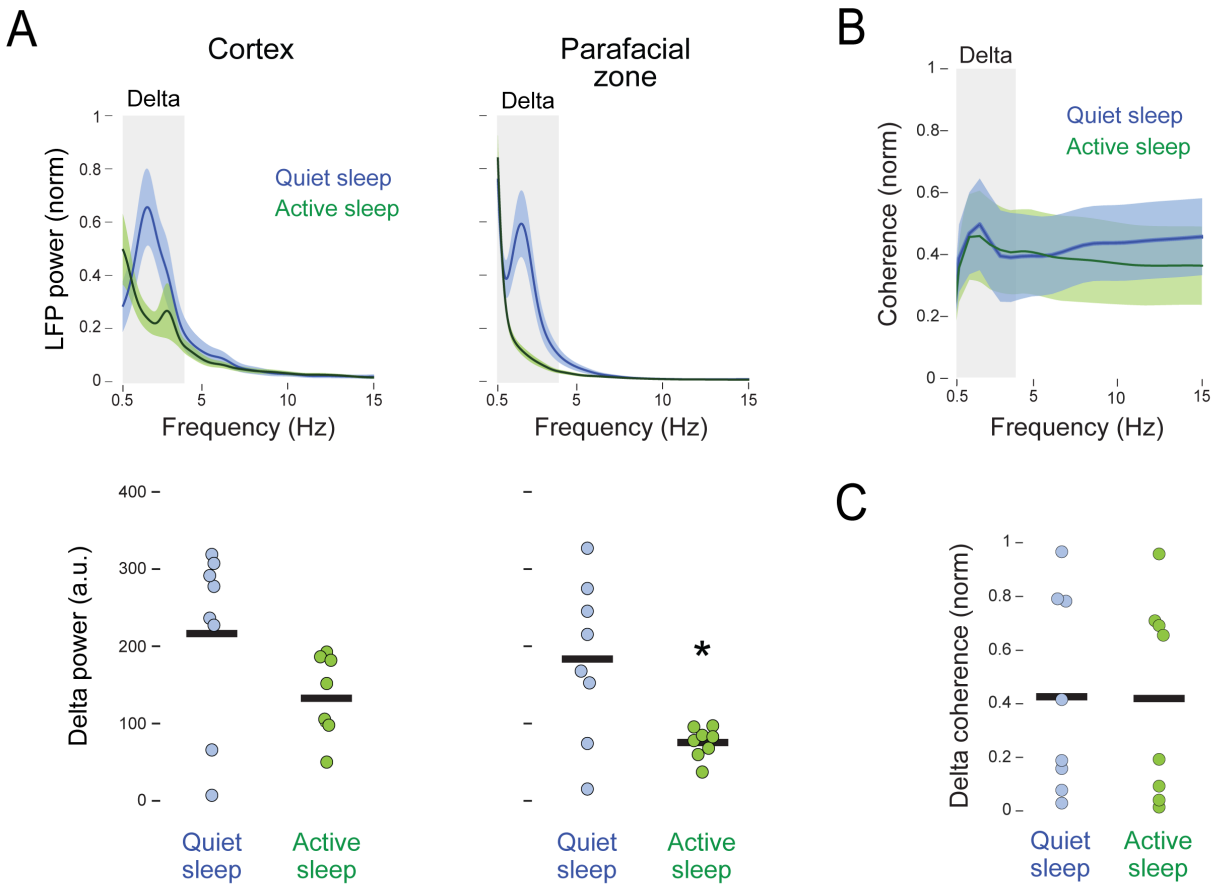

Figure 6. Delta rhythms in cortex and PZ are not coherent in P10 rats

(A) Top: Mean (± SEM) LFP power spectra for frontal cortex (left) and PZ (right) during quiet and active sleep. Gray zones indicate delta frequencies (0.5-4 Hz). Bottom: Mean power (arbitrary units, a.u.) within delta frequencies during quiet and active sleep. Data points show power for individual pups. Asterisk denotes significant difference between groups.

(B) Mean (± SEM) LFP coherence between frontal cortex and PZ during quiet and active sleep. Gray zone indicates delta frequencies (0.5-4 Hz).

(C) Mean normalized (norm) delta coherence for each pup during quiet and active sleep. Coherence values were normalized across both sleep states. Individual data points are average values for pups.

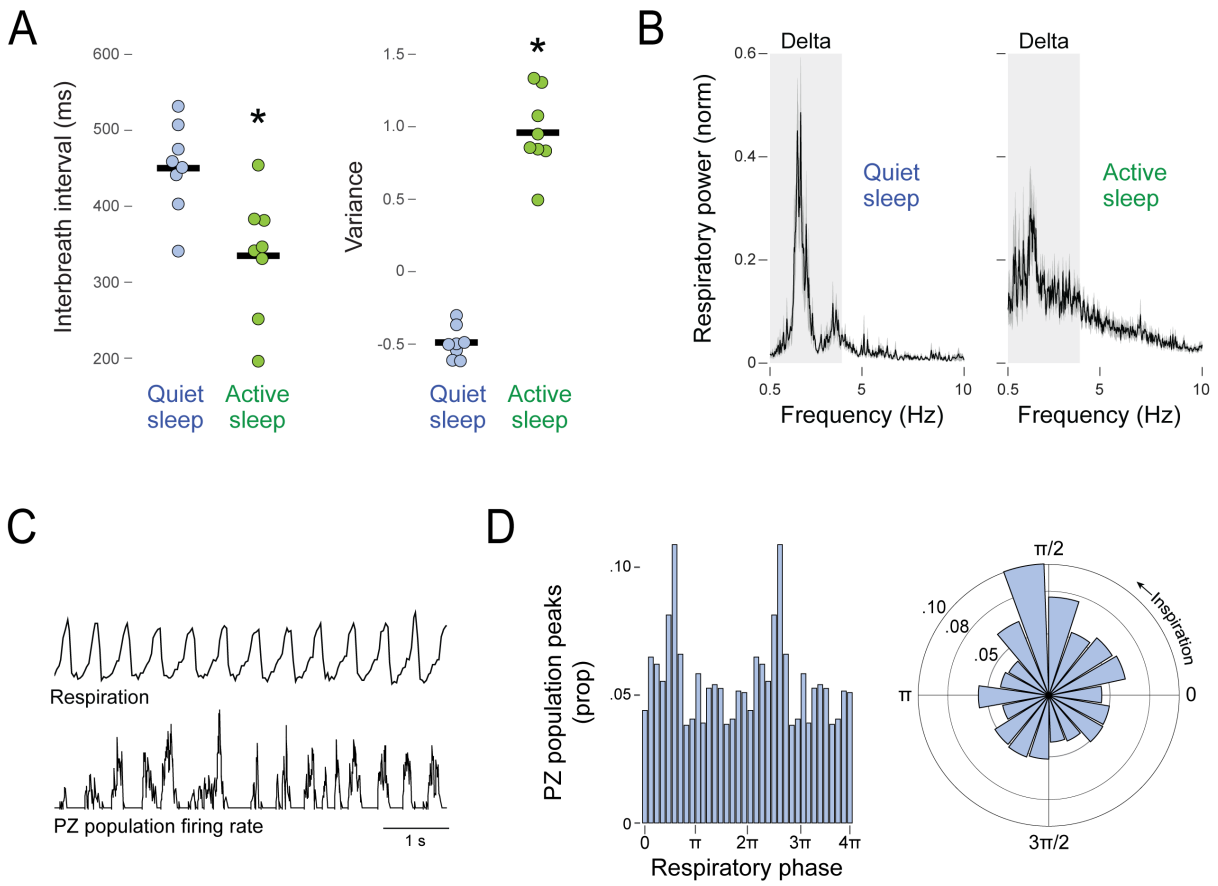

Figure 7. State-dependent modulation of respiration and respiratory modulation of PZ unit activity in P12 rats

(A) Mean inter-breath interval (left) and variance of instantaneous breathing rate (right) during quiet and active sleep. Individual data points are average values for pups. Asterisks denote significant difference between groups.

(B) Mean (± SEM) respiratory power spectra during quiet sleep (left) and active sleep (right). Gray zones indicate delta frequencies (0.5-4 Hz).

(C) Representative 6-s segment of data during quiet sleep showing a period of regular respiration (top) and associated rhythmic bursting of the population of PZ units (bottom).

(D) Left: Frequency distribution of mean proportion (prop) of PZ population peaks in relation to respiratory phase during quiet sleep. Note that the data are double-plotted. n = 8 pups. Right: Rose plot of the same data at left. The distribution is significantly non-uniform.

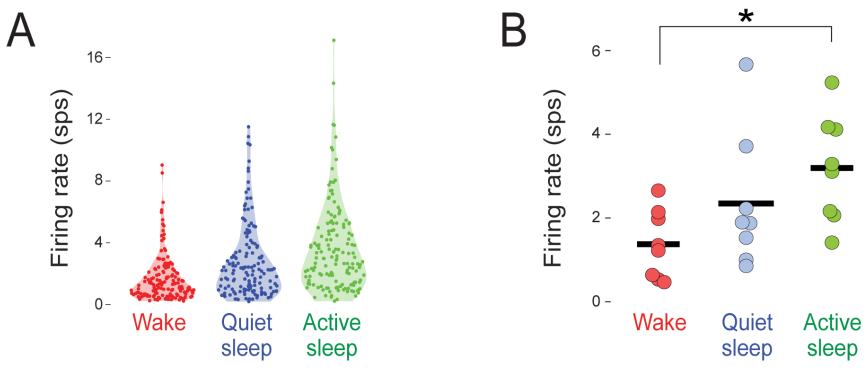

Figure S1. PZ unit firing rates across the sleep-wake cycle in P10 rats
(A) Violin plots showing mean firing rates (spikes/s) for all recorded single units during wake, quiet sleep, and active sleep.
(B). Mean firing rates (spikes/s) for each individual P10 rat during wake, quiet sleep, and active sleep. Individual data points are average values for pups. Asterisk denotes significant difference between the two groups.

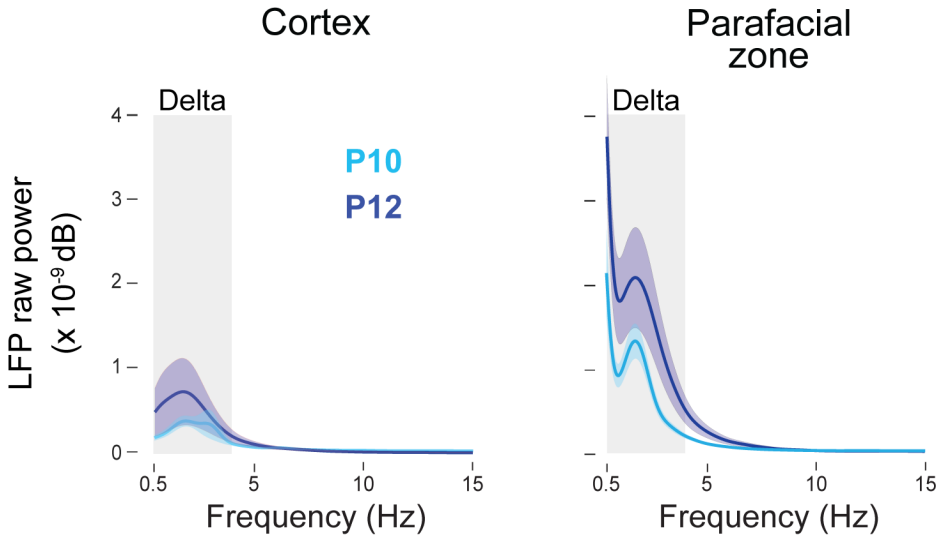

Figure S2. Developmental changes in raw power spectra at P12
Mean (± SEM) raw spectral power was computed in frontal cortex (left) and PZ (right) at P10 (n = 7) and P12 (n = 8). PZ delta was used to identify periods for analysis in both structures; however, the results were similar when cortical delta was used to define these periods (data not shown). Gray zones indicate delta frequencies (0.5-4 Hz).

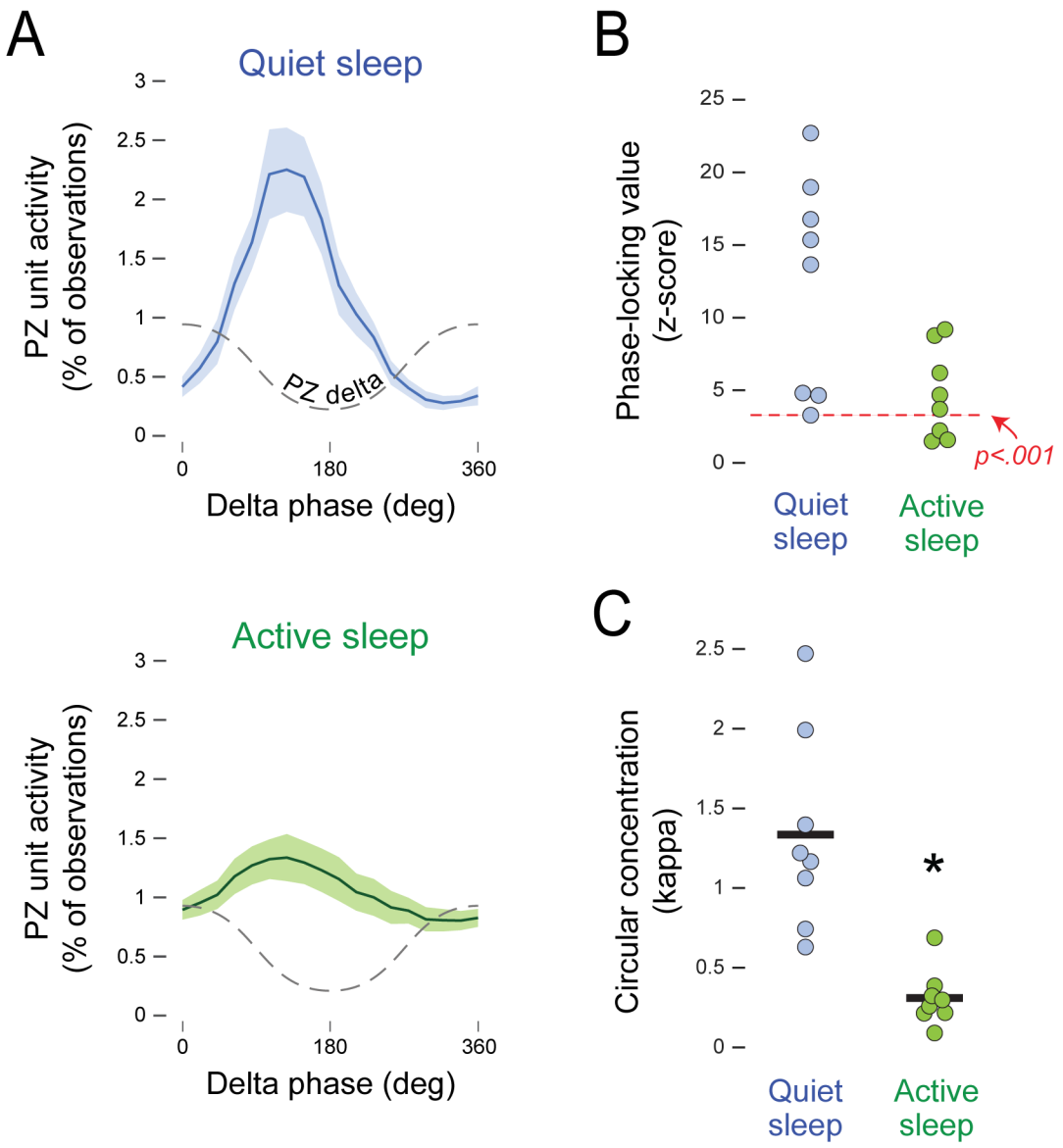

Figure S3. PZ units are phase-locked with delta in P10 rats

(A) Mean (± SEM) PZ unit activity in relation to delta phase in PZ during quiet sleep (top) and active sleep (bottom). Delta phase is illustrated with dashed lines.

(B) Phase-locking values (z-scored) of PZ unit activity in relation to local delta phase during quiet and active sleep. Individual data points are average values for pups. Red dotted line indicates a significance level of $p < .001$ based on a z-score of 3.29.

(C) Mean circular concentration coefficients (kappa) of PZ units in relation to local delta phase during quiet and active sleep. Individual data points are average values for pups. Asterisk denotes significant difference.

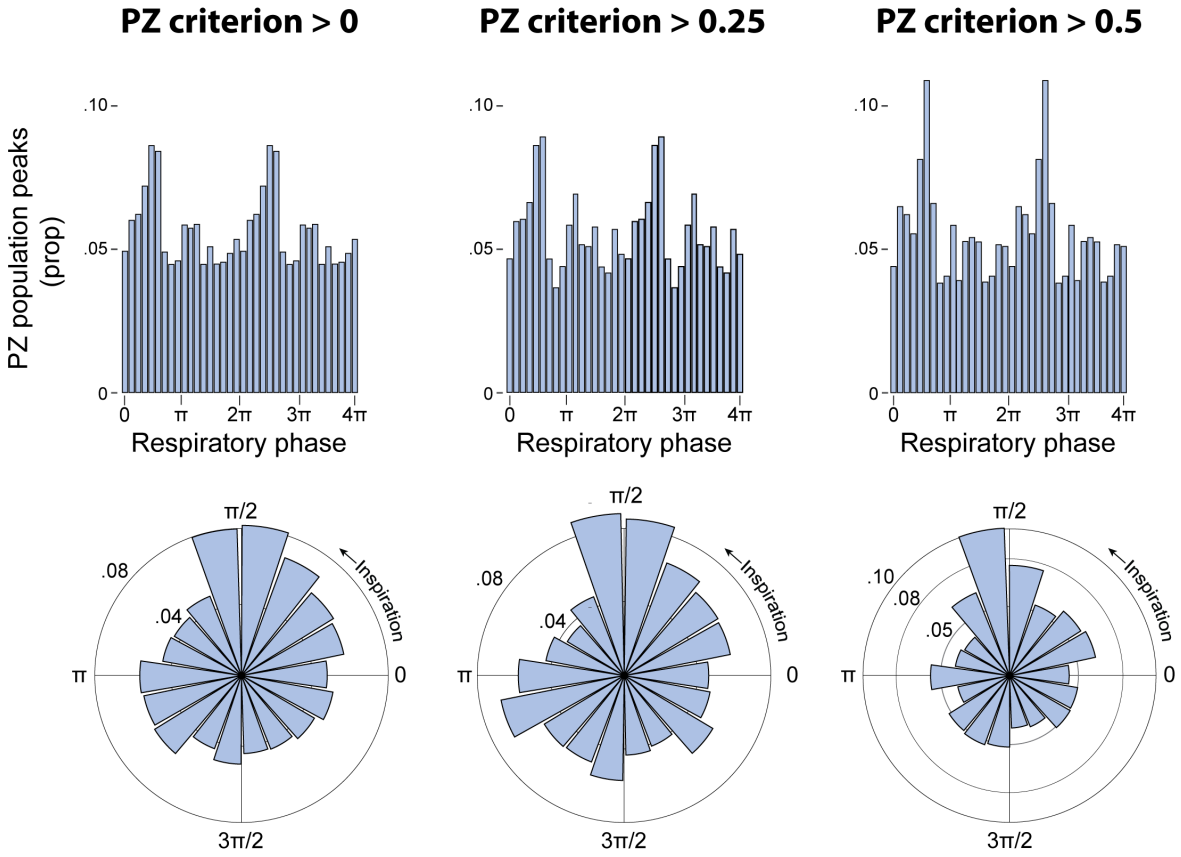

Figure S4. PZ population activity is phase-locked to respiration in P12 rats.
Top: Frequency distribution of mean proportion (prop) of PZ population peaks in relation to respiratory phase during quiet sleep. Note that the data are double-plotted. n = 8 pups. Bottom: Rose plots of the data above. Columns from left to right show results using increasingly stringent criteria for defining PZ bursting activity; the plots in the right-most column are the same as those in **Figure 7C**. The three distributions are significantly non-uniform (*Z*s $\geq$ 44.43, *p*s < .001).

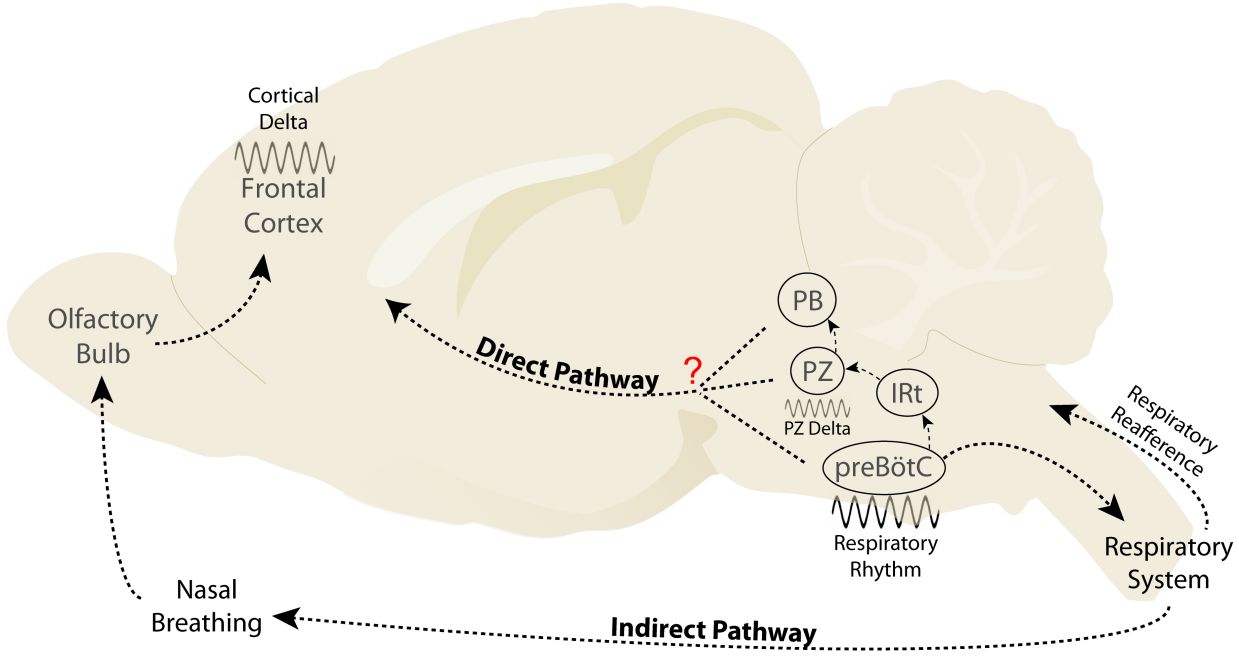

Figure S5. Possible mechanisms contributing to PZ and cortical delta in infant rats
Rhythmic spiking in the parafacial zone (PZ) may arise in similar fashion to the activity described for whisking in the intermediate reticular nucleus (IRt), a structure that also projects heavily to PZ. In turn, IRt receives input from the inspiratory pacemaker in the preBötzinger complex (preBötC), a component of the ventral respiratory group. PZ, preBötC, and the parabrachial nucleus (PB) have ascending projections that could directly influence how respiration modulates delta in frontal cortex. An indirect influence of respiration on cortical delta via nasal breathing and its effect on oscillatory activity in the olfactory bulbs is also thought to occur in adults, but elimination of that pathway in this study appears to rule it out as a factor at P12. Finally, the influence of sensory feedback (reafference) from respiratory muscles must also be considered. Figure adapted from Karalis and Sirota, 2022.[25]

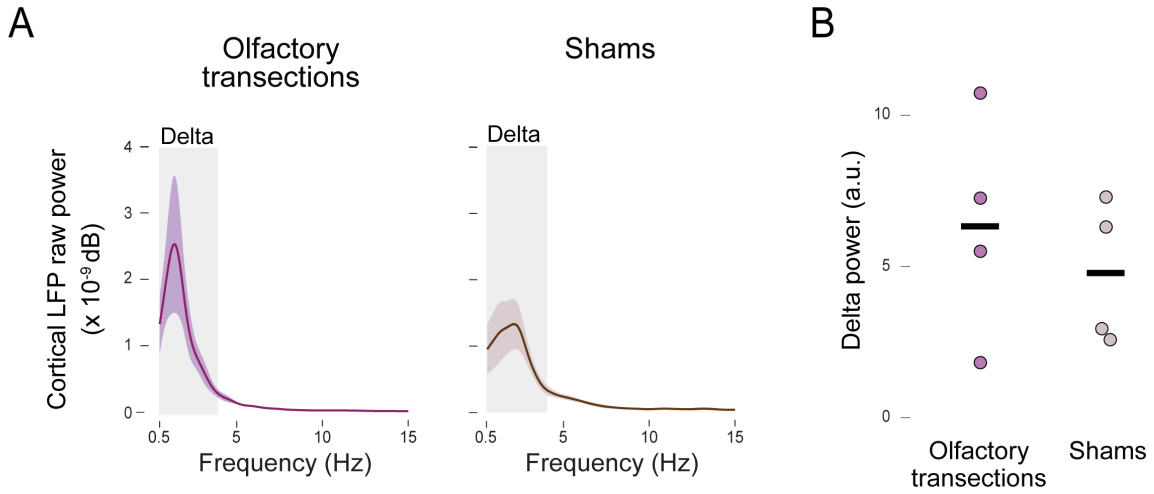

Figure S6. Disconnecting the main olfactory bulbs from the cortex at P12 does not diminish cortical delta power during quiet sleep

(A) Mean (± SEM) raw cortical power in P12 rats after bilateral transection of the lateral olfactory tract (left; n = 4) or sham transection (right; n = 4). Gray zones indicate delta frequencies (0.5-4 Hz).

(B) Mean power (arbitrary units, a.u.) within delta frequencies for pups after olfactory or sham transection. Data points show power for individual pups.

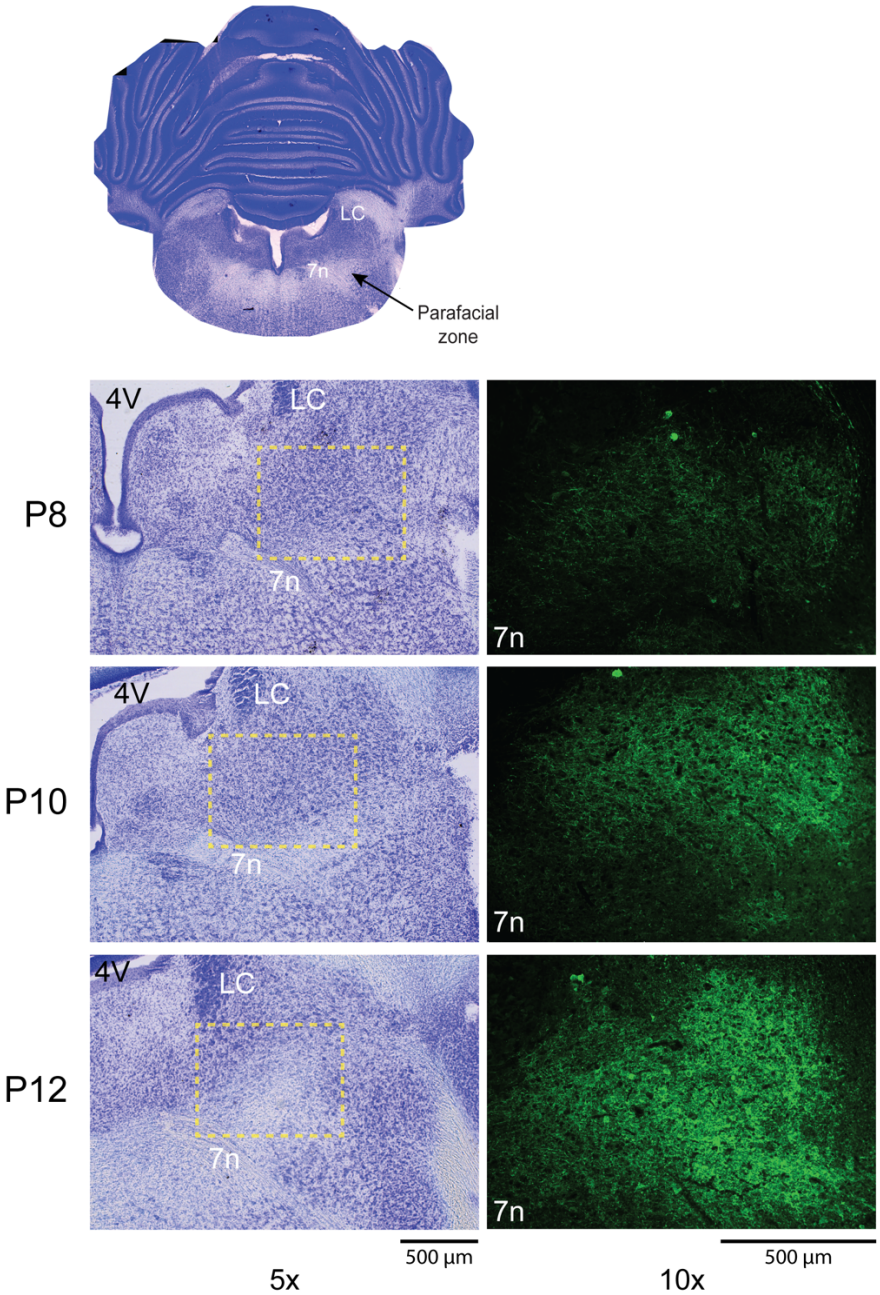

Figure S7. Increasing PV-expression in PZ between P8 and P12

(A) Coronal section of brain of infant rat, showing the location of PZ immediately dorsal to the facial nerve (7n) and ventral to the locus coeruleus (LC).

(B) Left column: Nissl-stained sections at 5x showing the region around PZ at P8 (top row), P10 (middle row), and P12 (bottom row). Dashed yellow boxes outline the regions shown at right: Right column: Representative sections at 10x showing PV-expressing terminals in PZ at the three ages. The exposure and gain were standardized across ages to enable age-related comparisons in expression. 4V, 4th ventricle.

STAR METHODS

RESOURCE AVAILABILITY

Lead Contact

Further information and requests for resources should be directed to, and will be fulfilled by, the lead contact, Dr. Mark Blumberg (mark-blumberg@uiowa.edu).

Materials Availability

This study did not generate new unique reagents.

Data and Code Availability

Electrophysiological spiking and LFP data, respiratory data, as well as time codes for states for each animal will be deposited at Dryad for public availability by the date of publication. All original code has been deposited at https://github.com/Blumberg-Lab/Ahmad-et-al.-2024 and is publicly available.

Any additional information required to reanalyze the data reported in this paper is available from the lead contact upon request.

EXPERIMENTAL MODEL AND SUBJECT DETAILS

Male and female Sprague-Dawley Norway rats *(Rattus norvegicus)* at postnatal day (P) 8, P10, and P12-13 (hereafter P12) were used. Pups were housed and reared in standard laboratory cages (48 x 20 x 26 cm) under 12-h light/dark cycles; food and water were available *ad libitum*. Littermates were always assigned to different experimental groups to avoid litter effects and associated inflation of statistical power.[69,70] Litters were culled to eight pups by P3. All experiments were performed in compliance with the National Institutes of Health *Guide for the Care and Use of Laboratory Animals* (NIH Publication No. 80–23) and were approved by the Institutional Animal Care and Use Committee at the University of Iowa.

PZ and cortical activity were recorded at P10 (n = 8; 5 males; body weight = 23.31 $\pm$ 2.47 g) and P12 (n = 8; 4 males; body weight = 29.67 $\pm$ 1.41 g). In a separate cohort of pups, PZ and cortical activity were recorded at P12 after bilateral transection of the lateral olfactory tract (n = 4 pups; 2 males; body weight = 26.25 $\pm$ 0.83 g) or sham transection (n = 4 pups; 2 males; body weight = 26.41 $\pm$ 0.61 g). Finally, PV expression was assessed in rats at P8 (n = 4; 2 males; body weight = 19.2 + 1.1 g), P10 (n = 3; 2 males; body weight = 22.9 + 1.5 g), and P12 (n = 4; 1 male; body weight = 27.2 + 2.3 g).

METHOD DETAILS

Surgery and Experimental Procedures

Neural activity in PZ and cortex across behavioral states in P10 and P12 rats. PZ and cortical activity were recorded from unmanipulated rat pups at P10 and P12. As described previously,[71,72] on the day of testing a pup with a visible milk-band was removed

from the litter and anesthetized (3-5% isoflurane gas; Phoenix Pharmaceuticals, Burlingame, CA). The pup was placed on a heating pad for the duration of surgery to maintain body temperature. The scalp was swabbed with iodine and alcohol, and an anti-inflammatory analgesic (Carprofen, 5mg/kg; Putney, Portland, ME) was injected subcutaneously. The scalp was removed and a topical analgesic (bupivacaine, Pfizer, New York, NY) was applied to the skull. Bleach was subsequently applied with an applicator to dry the skull. To prevent bleeding, Vetbond (3M, Minneapolis, MN) was applied around the incision. Two custom-made stainless steel bipolar hook electrodes (50 µm diameter; California Fine Wire, Grover Beach, CA) were inserted into the left and right nuchal muscles and secured with collodion. The pup's torso was wrapped in soft surgical tape (Micropore, 3M) and, to measure respiration, a piezoelectric sensor (Unimed Electrode Supplies, Surrey, UK) was secured with additional soft tape to the back. Next, the pup's skull was secured to a stainless-steel head-fix (Neurotar, Helsinki, Finland) using cyanoacrylate adhesive (Loctite, Henkel Corporation, Westlake, OH) and an accelerant (Insta-Set, Bob Smith Industries, Atascadero, CA).

The pup was secured to a stereotaxic apparatus where anesthesia was maintained. Holes in the skull were drilled to enable subsequent electrode placement in PZ (relative to lambda, P10: +1.80 mm rostrocaudal (RC), 1.50 mm mediolateral (ML); P12: +1.80 mm RC, 1.70-1.80 mm ML) and secondary motor cortex (M2; relative to bregma, P10/12: +1.0 mm RC, 1.8–2.0 mm ML). A small hole was drilled over the contralateral parietal cortex for the insertion of a fine-wire thermocouple (Omega Engineering, Stamford, CT) during acclimation and a ground/reference electrode during recording. The ground/reference was a chlorinated silver wire (Ag/AgCl; 0.25 mm diameter, Medwire, Mt. Vernon, NY). Mineral oil was applied to the cortical surface to prevent drying. The duration of the entire surgical procedure was approximately 30 min.

After surgery, the pup was secured to the head-fix apparatus inside a grounded Faraday cage. The pup's torso was secured using surgical tape to an elevated narrow platform, with limbs dangling freely on each side (**Figure 1A**). Brain temperature was monitored to ensure that it was maintained at 36-37˚C; also, the local environment was humidified using moist sponges placed beneath the pup. The pup acclimated to the recording chamber for at least 1 h, and recording did not begin until regular sleep-wake cycles were observed. After acclimation, the thermocouple was replaced with the ground electrode. At that time, data acquisition began and electrophysiological, respiratory, and video data were recorded for at least 1 h.

Cortical delta power during QS after disconnection of the olfactory bulbs from the cortex. PZ and cortical activity were recorded from P12 rats after bilateral transection of the lateral olfactory tract (n = 4) or sham transection (n = 4), as described previously.[73] All surgical procedures were identical to those described above, except that the olfactory tracts were transected before the head-fix was attached. Briefly, transections were performed by inserting a 25 G needle through the skull, to the left and right of midline and at the level of the orbits. The needle was inserted perpendicularly until it touched the bottom of the skull and then swept using a side-to-side motion. For sham transections, only the two holes were made. After 90 min of recovery in an incubator maintained at 36˚C, the pup was moved to the recording apparatus and electrodes were inserted into

PZ and cortex. After at least 1 h and when regular sleep-wake cycles were observed, electrophysiological, respiratory, and video data were recorded for at least 1 h.

Electrophysiological Recordings

Neurophysiological and respiratory data were acquired using a data acquisition system (LabRat LR-10; Tucker-Davis Technologies, Alachua, FL). For both recording experiments, PZ data were obtained using a small-site 16-channel linear silicon electrode (Model A1x16-10 mm-100-177-A16; NeuroNexus, Ann Arbor, MI); before insertion, the electrode was coated with fluorescent DiI (Vybrant DiI Cell-Labeling Solution, Invitrogen, Waltham, MA) for subsequent histological verification. PZ electrodes were inserted at a depth of 4.3-4.8 mm. For cortical LFP recordings, a large-site 16-channel linear silicon electrode (Model A1x16-3 mm-100-703-A16; NeuroNexus) was coated with DiI and inserted into M2 at a depth of 0.6–1 mm. Neural signals from the electrodes were sampled at ~25 kHz using a high-pass filter (0.1 Hz) and a harmonic notch filter (60, 120, and 180 Hz). Respiratory data were sampled at ~30 Hz.

Video Recording and Synchronization

As described previously,[49] videos of body and limb movements were recorded using a digital video camera (Blackfly-S, 100 frames/s, 3000-ms exposure, 720 x 540 pixel resolution, FLIR Integrated Systems, Wilsonville, OR) and acquired using SpinView software (FLIR). The video was synchronized to the electrophysiological data using an LED visible within the camera frame that automatically pulsed every 3 s for 100 ms. After acquisition, if frames were dropped between LED pulses, a custom MATLAB script was used to insert blank frames.[74]

Histology

After recording, the pup was euthanized with ketamine/xylazine (10:1, >0.08 mg/kg IP) and perfused with 0.1 M PBS followed by 4% paraformaldehyde. The brain was extracted and fixed in 4% paraformaldehyde for at least 24 h, after which it was transferred to a 30% sucrose phosphate-buffered solution for another 24-48 h before sectioning. The hindbrain was sectioned coronally at 80 μm using a freezing microtome (Leica Biosystems, Buffalo Grove, IL) and mounted on gelatin-coated slides. Electrode tracks were confirmed using a fluorescent microscope (2.5-5x magnification, Leica Microsystems, Deerfield, IL). Slides were subsequently Nissl-stained using Cresyl violet. Electrode placements were confirmed by overlaying the fluorescent image onto a Nissl-stained image of the same section. For pups with bilateral transection of the lateral olfactory tract, the brain was extracted from the skull to confirm that the main olfactory bulbs were completely disconnected from the cortex.

Pre-Processing of Neural Data

Neural data were preprocessed using custom MATLAB scripts.[49,75,76] Briefly, to analyze LFPs from PZ and cortex, raw neural activity were downsampled to ~1000 Hz, smoothed using a .005 s moving Gaussian kernel, and converted to binary files. For unit activity in PZ, raw neural activity was bandpass filtered (300-5000 Hz) and converted to binary files. Putative units were acquired from templates extracted using Kilosort[77] and visualized and

confirmed using Phy2.[78] Waveforms and waveform autocorrelations were used to identify single units and multi-units (hereafter referred to as units). Sorted units, LFPs, movement data, and respiratory waveforms were imported into Spike2 (Cambridge Electronic Design, Cambridge, UK) or MATLAB for analysis.

Classification of Behavioral State

Behavioral state was classified using a combination of respiratory, movement, and LFP data.[11,21,22,74] As a first step in this process, the respiratory signal was examined for periods with large movement artifacts. Periods where the amplitude of the respiratory signal was 2 standard deviations (SDs) above or below the median were excluded from analysis. To distinguish periods of regular and irregular breathing, respiratory data were analyzed by adapting a previously described method.[22] Briefly, respiratory peaks were used to derive inter-breath intervals, and these intervals were inverted to obtain the instantaneous breathing rate. Variance of instantaneous breathing rate was computed in 2-s windows and the variances were z-transformed. The 75th percentile was used as a threshold such that values below the threshold identified periods of regular breathing, and values above the threshold identified periods of irregular breathing (consistent with QS and AS, respectively).

Limb movements were detected using a custom MATLAB script that identified changes in pixel intensity between video frames within regions-of-interest (ROIs: forelimbs, hindlimbs, whole-body), producing an output of real-time movement.[74]

Active wake was identified as periods when multiple body parts exhibited coordinated and high-amplitude movements. When a transition to QS occurred, respiration was regular and limb movements were absent. In addition, periods of delta were identified when cortical and PZ LFPs, filtered for delta (0.5-4 Hz), increased above the median LFP amplitude. At P12, both cortical and PZ LFPs were used to define periods of delta; however, because cortical delta was less reliable at P10, only the PZ LFP was used to define periods of delta at this age. AS began with the onset of limb twitching, irregular respiration, and the cessation of cortical and/or PZ delta. If a train of twitches was followed by 10 s of silence, then the AS period ended with the last twitch observed. Finally, periods of wake, QS, and AS were required to be at least 3 s in duration to be analyzed.

PV Immunohistochemistry

Brain slices from pups at P8 (n = 4), P10 (n = 3), and P12 (n = 4) were used for PV staining. Brains were sliced in 50 μm sections, with one section used for PV staining and the adjacent section used for Nissl staining. Sections were mounted on gelatin-coated slides and allowed to dry for at least 90 min. Slides were rehydrated in distilled water for 1 min and then permeabilized in 0.2% triton in PBS for 10 min. Slides were washed 3 times for 5 min in PBS, then blocked in 3% BSA blocking buffer (Thermo Scientific, Waltham, MA) with 5% donkey serum (Equitech-Bio, Kervville,TX) for 2 h. Primary antibody against PV (PV27a; Swant, Burgdorf, Switzerland) was diluted 1:100 in blocking buffer and applied to the sections, which were then incubated for 48 h at 4°C. After primary incubation, the slides were washed 3 times in PBS. Secondary antibody (Alexa Fluor 488 donkey anti-rabbit IgG; Life Technologies, Grand Island, NY) was diluted 1:500

in PBS and applied to the sections; sections were then incubated for 90 min at room temperature. The slides were cover-slipped using Prolong Gold (Invitrogen) and expression of PV was visualized and imaged using a fluorescent microscope (Leica).

QUANTIFICATION AND STATISTICAL ANALYSIS

All statistical analyses were conducted using either SPSS 29 (IBM, Armonk, NY) or MATLAB. Statistical tests included repeated-measures ANOVA, paired t tests, and Rayleigh tests. Data were tested for normality using the Shapiro-Wilks test. When appropriate, Mauchly's test was used to test for sphericity. In analyses where sphericity was violated, a Huynh-Feldt correction was applied to the degrees of freedom. Bonferroni corrections were used when appropriate to adjust alpha for multiple comparisons. The measure of effect size was partial eta-squared (adjusted for positive bias[79]) for ANOVAs, and as Hedge's g for paired t tests. Unless otherwise stated, mean data are always presented with their standard error (SEM). Outlier values that were 3 SDs above or below the mean were excluded from analysis; this occurred only once.

PZ Firing Rate

To determine if PZ activity was modulated by behavioral state, the average firing rate was calculated for each unit during each state. Unit firing rates were averaged within each pup before statistical analysis.

For identifying periods of PZ silence, a custom MATLAB script was used to concatenate unit activity within each pup. Using the concatenated record, silent periods were identified when there was a complete absence of activity for at least 50 ms. Normalized frequency histograms of 5-ms bins were then generated to show the distribution of silent periods during each state. Values for each time bin were average across pups. The proportion of 5-ms bins between 0.1 and 0.5 s during each state was then computed.

LFP Power Spectra and Coherence in PZ and Cortex

For analysis of LFPs, one electrode channel in PZ and cortex was selected from each pup. Channels were selected based on their location in each region and their raw delta amplitude. In the cortex, higher-amplitude LFPs occurred in the shallower channels.

The MATLAB function, "pspectrum()," was used to generate raw power spectra. A sampling frequency of 1000 Hz was used, and spectral values between 0.5 and 30 Hz were calculated and normalized within pups across states. The normalized power spectral values were then averaged across pups. One cortical LFP at P12 was excluded due to noise contamination. Finally, the area under the curve within delta frequencies was calculated for each pup to compare delta power between QS and AS.

For generating raw power spectra in olfactory-tract-transected and sham-transected pups, approximately 30-s periods of QS were chosen during which respiration was regular and cortical LFPs (filtered for delta) were above the median amplitude (calculated across the entire recording). These periods were used to generate raw power spectra and delta power, as described above.

For calculating LFP-LFP coherence, we used custom MATLAB scripts.[27,80] The raw LFPs were bandpass-filtered (0 -.5 Hz) to remove DC components. Each LFP signal was then convolved using a complex Morlet wavelet. To create the Morlet wavelet, the frequency band of interest (0.5-30 Hz) was divided into 50 bins. The temporal resolution of the wavelet was defined using a minimum of 4 cycles and a maximum of 8 cycles. A sampling frequency of 1000 Hz was used, and coherence was generated on a linear scale.

Coherence was computed as follows:

$$Coherence_{xy} = \frac{S_{xy}}{S_{xx} \times S_{yy}}$$

where S_{xy} is the cross-spectral density between signals X and Y, and S_{xx} and S_{yy} are the auto-spectral densities (i.e., the average power).

Cross-spectral density was computed as follows:

$$S_{xy} = |n^{-1} \sum_{t=1}^{n} |X_{tf}||Y_{tf}|e^{i\varphi t_{xy}}|$$

where S_{xy} contains the complex-valued coherence. At a specific frequency (f) and a given time (t), the magnitude of signals X and Y and their phase differences following Euler's formula ($e^{i\varphi}$) were computed to obtain the average of magnitude-modulated phase values. For auto-spectral density, all the computations were the same, except the same LFPs were used twice.

Coherence values between cortical and PZ delta (0.5-4 Hz), as calculated above, were normalized within each pup across states, and then averaged across pups. One P12 pup was excluded from the analysis due to a noisy cortical LFP, and another was excluded as an outlier.

Phase Locking of PZ Unit Activity with Local Delta

Phase-locking values (PLVs) for PZ units were computed using custom MATLAB scripts.[27,81,82] Briefly, the phases of the bandpass-filtered (0.5-4 Hz) LFPs were extracted using Hilbert transform. Spike trains for each unit were used to generate spike-phase distributions (phase bin size = 20°); for each LFP phase, the occurrences of spikes were counted and then divided by the total number of spikes.

Rayleigh tests were used to determine significant PLVs.[81] First, phase estimates were assigned to each index of spike times, and a phase histogram was extracted for each

spike. PLVs were computed and z-transformed by bootstrap shuffling (n = 1000 iterations). To do this, a random LFP point was selected and segments on either side of that point were shuffled.

The circular concentration coefficient (kappa; κ) was calculated using the von Mises probability distribution.[28] The probability density function under this distribution was calculated as follows:

$$Probability_{\alpha;\mu,\kappa} = \frac{\exp(\kappa\cos(\alpha - \mu)}{2\pi\, I_0(\kappa)}$$

where α is the angular direction, μ is a measure of location (i.e., clustering around μ), and I_0 is the modified Bessel function of order zero. A higher κ indicates that the PLVs were more likely to be concentrated at specific phases of delta.

Respiratory Modulation of PZ Unit Activity

Inter-breath intervals and variance of instantaneous breathing rate were calculated as described above for each P12 rat during QS and AS. The spectral power of the respiratory rhythm was generated as described for LFP, normalized across state, and then averaged across pups.

For capturing the respiratory modulation of PZ population firing rate at P12, the average firing rate across all PZ units within a pup was calculated using 1-ms bins. Next, the average PZ firing rate was smoothed using a 5-ms moving window. The values exceeding a criterion were used to generate PLVs of the PZ population firing rate in relation to the respiratory rhythm. Three increasingly conservative criteria were used: 0 x median (no threshold), .25 x median, and .50 x median. PLVs were generated as described above for LFPs, but here the PZ population firing rate was used instead of individual PZ units. The population PZ peaks were mapped along the oscillatory respiratory phases (20°/bin) to generate histograms and rose plots.

References

1. Buzsáki, G. (2006). Rhythms of the brain (Oxford University Press).

2. Buzsáki, G., Logothetis, N., and Singer, W. (2013). Scaling brain size, keeping timing: evolutionary preservation of brain rhythms. Neuron *80*, 751–764. 10.1016/j.neuron.2013.10.002.

3. Winfree, A. (1987). The timing of biological clocks (Scientific American Library).

4. Kleinfeld, D., Deschênes, M., Wang, F., and Moore, J.D. (2014). More than a rhythm of life: breathing as a binder of orofacial sensation. Nat Neurosci *17*, 647–651. 10.1038/nn.3693.

5. Puentes-Mestril, C., Roach, J., Niethard, N., Zochowski, M., and Aton, S.J. (2019). How rhythms of the sleeping brain tune memory and synaptic plasticity. Sleep *42*, zsz095. 10.1093/sleep/zsz095.

6. Adamantidis, A.R., Herrera, C.G., and Gent, T.C. (2019). Oscillating circuitries in the sleeping brain. Nat Rev Neurosci *20*, 746–762. 10.1038/s41583-019-0223-4.

7. Borb, A.A., and Achermann, P. (1999). Sleep Homeostasis and Models of Sleep Regulation. J. Biol. Rhythm. *14*, 559–570. 10.1177/074873099129000894.

8. Girardeau, G., and Lopes-dos-Santos, V. (2021). Brain neural patterns and the memory function of sleep. Science *374*, 560–564. 10.1126/science.abi8370.

9. Crunelli, V., Lőrincz, M.L., Connelly, W.M., David, F., Hughes, S.W., Lambert, R.C., Leresche, N., and Errington, A.C. (2018). Dual function of thalamic low-vigilance state oscillations: rhythm-regulation and plasticity. Nat Rev Neurosci *19*, 107–118. 10.1038/nrn.2017.151.

10. Rasch, B., and Born, J. (2013). About sleep's role in memory. Physiol Rev *93*, 681–766. 10.1152/physrev.00032.2012.

11. Seelke, A.M.H., and Blumberg, M.S. (2008). The microstructure of active and quiet sleep as cortical delta activity emerges in infant rats. Sleep *31*, 691–699.

12. Frank, M., and Heller, H. (1997). Development of REM and slow wave sleep in the rat. Am J Physiol *272*, R1792–R1799.

13. Jouvet-Mounier, D., Astic, L., and Lacote, D. (1970). Ontogenesis of the states of sleep in rat, cat, and guinea pig during the first postnatal month. Dev Psychobiol *2*, 216–239. 10.1002/dev.420020407.

14. Gramsbergen, A., Schwartze, P., and Prechtl, H.F.R. (1970). The postnatal development of behavioral states in the rat. Dev Psychobiol *3*, 267–280.

15. Anaclet, C., and Fuller, P.M. (2017). Brainstem regulation of slow-wave-sleep. Curr Opin Neurobiol *44*, 139–143. 10.1016/j.conb.2017.04.004.

16. Villablanca, J.R. (2004). Counterpointing the functional role of the forebrain and of the brainstem in the control of the sleep–waking system. J Sleep Res *13*, 179–208.

17. Anaclet, C., Pedersen, N.P., Ferrari, L.L., Venner, A., Bass, C.E., Arrigoni, E., and Fuller, P.M. (2015). Basal forebrain control of wakefulness and cortical rhythms. Nat Commun *6*, 8744. 10.1038/ncomms9744.

18. Anaclet, C., Lin, J.S., Vetrivelan, R., Krenzer, M., Vong, L., Fuller, P.M., and Lu, J. (2012). Identification and characterization of a sleep-active cell group in the rostral medullary brainstem. J Neurosci *32*, 17970–17976. 10.1523/jneurosci.0620-12.2012.

19. Alam, M.A., Kostin, A., Siegel, J., McGinty, D., Szymusiak, R., and Alam, M.N. (2018). Characteristics of sleep-active neurons in the medullary parafacial zone in rats. Sleep *41*. 10.1093/sleep/zsy130.

20. Anaclet, C., Ferrari, L., Arrigoni, E., Bass, C.E., Saper, C.B., Lu, J., and Fuller, P.M. (2014). The GABAergic parafacial zone is a medullary slow wave sleep–promoting center. Nat Neurosci *17*, 1217–1224. 10.1038/nn.3789.

21. Saini, J.K., and Pagliardini, S. (2017). Breathing during sleep in the postnatal period of rats: The contribution of active expiration. Sleep *40*, 1071–13. 10.1093/sleep/zsx172.

22. Isler, J.R., Thai, T., Myers, M.M., and Fifer, W.P. (2016). An automated method for coding sleep states in human infants based on respiratory rate variability. Dev Psychobiol *58*, 1108–1115. 10.1002/dev.21482.

23. Biskamp, J., Bartos, M., and Sauer, J.-F. (2017). Organization of prefrontal network activity by respiration-related oscillations. Sci Rep *7*, 45508. 10.1038/srep45508.

24. Tort, A.B.L., Brankačk, J., and Draguhn, A. (2018). Respiration-entrained brain rhythms are global but often overlooked. Trends Neurosci *41*, 186–197. 10.1016/j.tins.2018.01.007.

25. Karalis, N., and Sirota, A. (2022). Breathing coordinates cortico-hippocampal dynamics in mice during offline states. Nat Commun *13*, 467. 10.1038/s41467-022-28090-5.

26. Tort, A.B.L., Ponsel, S., Jessberger, J., Yanovsky, Y., Brankačk, J., and Draguhn, A. (2018). Parallel detection of theta and respiration-coupled oscillations throughout the mouse brain. Sci Rep *8*, 6432. 10.1038/s41598-018-24629-z.

27. Rio-Bermudez, C.D., Kim, J., Sokoloff, G., and Blumberg, M.S. (2017). Theta oscillations during active sleep synchronize the developing rubro-hippocampal sensorimotor network. Curr Biol *27*, 1413–1424. 10.1016/j.cub.2017.03.077.

28. Berens, P., and Velasco, M. (2009). The circular statistics toolbox for Matlab. MPI Tech Rep *184*.

29. Buzsáki, G., and Vöröslakos, M. (2023). Brain rhythms have come of age. Neuron *111*, 922–926. 10.1016/j.neuron.2023.03.018.

30. Schnitzler, A., and Gross, J. (2005). Normal and pathological oscillatory communication in the brain. Nat Rev Neurosci *6*, 285–296. 10.1038/nrn1650.

31. Takatoh, J., Prevosto, V., Thompson, P.M., Lu, J., Chung, L., Harrahill, A., Li, S., Zhao, S., He, Z., Golomb, D., et al. (2022). The whisking oscillator circuit. Nature *609*, 560–568. 10.1038/s41586-022-05144-8.

32. Anaclet, C., Lin, J.-S., Vetrivelan, R., Krenzer, M., Vong, L., Fuller, P.M., and Lu, J. (2012). Identification and characterization of a sleep-active cell group in the rostral medullary brainstem. J Neurosci *32*, 17970–17976. 10.1523/jneurosci.0620-12.2012.

33. Gervasoni, D., Lin, S.-C., Ribeiro, S., Soares, E.S., Pantoja, J., and Nicolelis, M.A.L. (2004). Global forebrain dynamics predict rat behavioral states and their transitions. J Neurosci *24*, 11137–11147. 10.1523/jneurosci.3524-04.2004.

34. Villablanca, J., Andrés, I.D., and Olmstead, C. (2001). Sleep-waking states develop independently in the isolated forebrain and brain stem following early postnatal midbrain transection in cats. Neuroscience *106*, 717–731.

35. Batini, C., Palestini, M., Rossi, G.F., and Zanchetti, A. (1959). EEG activation patterns in the mid-pontine pretrigeminal cat following sensory deafferentation. Arch Ital Biol *97*, 26–32.

36. Cordeau, J.P., and Mancia, M. (1959). Evidence for the existence of an electroencephalographic synchronization mechanism originating in the lower brain stem. Electroencephalogr. Clin. Neurophysiol. *11*, 551–564. 10.1016/0013-4694(59)90054-9.

37. Batini, C., Moruzzi, G., Palestini, M., Rossi, G.F., and Zanchetti, A. (1958). Persistent patterns of wakefulness in the pretrigeminal midpontine preparation. Science *128*, 30–32. 10.1126/science.128.3314.30-b.

38. Negro, C.A.D., Funk, G.D., and Feldman, J.L. (2018). Breathing matters. Nat Rev Neurosci *19*, 351–367. 10.1038/s41583-018-0003-6.

39. Lohmann, C., and Friauf, E. (1996). Distribution of the calcium-binding proteins parvalbumin and calretinin in the auditory brainstem of adult and developing rats. J Comp Neurol *367*, 90–109. 10.1002/(sici)1096-9861(19960325)367:1<90::aid-cne7>3.0.co;2-e.

40. Alcántara, S., Ferrer, I., and Soriano, E. (1993). Postnatal development of parvalbumin and calbindin D28K immunoreactivities in the cerebral cortex of the rat. Anat Embryol *188*, 63–73. 10.1007/bf00191452.

41. Kaila, K., Price, T.J., Payne, J.A., Puskarjov, M., and Voipio, J. (2014). Cation-chloride cotransporters in neuronal development, plasticity and disease. Nat Rev Neurosci *15*, 637–654. 10.1038/nrn3819.

42. Virtanen, M.A., Uvarov, P., Mavrovic, M., Poncer, J.C., and Kaila, K. (2021). The multifaceted roles of KCC2 in cortical development. Trends Neurosci *44*, 378–392. 10.1016/j.tins.2021.01.004.

43. Khazipov, R., Khalilov, I., Tyzio, R., Morozova, E., Ben-Ari, Y., and Holmes, G.L. (2004). Developmental changes in GABAergic actions and seizure susceptibility in the rat hippocampus. Eur J Neurosci *19*, 590–600.

44. Rivera, C., Voipio, J., Payne, J.A., Ruusuvuori, E., Lahtinen, H., Lamsa, K., Pirvola, U., Saarma, M., and Kaila, K. (1999). The K+/Cl- co-transporter KCC2 renders GABA hyperpolarizing during neuronal maturation. Nature *397*, 251–255. 10.1038/16697.

45. Marcano-Reik, A.J., Prasad, T., Weiner, J.A., and Blumberg, M.S. (2010). An abrupt developmental shift in callosal modulation of sleep-related spindle bursts coincides with the emergence of excitatory-inhibitory balance and a reduction of somatosensory cortical plasticity. Behav Neurosci *124*, 600–611.

46. Alfonsa, H., Burman, R.J., Brodersen, P.J.N., Newey, S.E., Mahfooz, K., Yamagata, T., Panayi, M.C., Bannerman, D.M., Vyazovskiy, V.V., and Akerman, C.J. (2023). Intracellular chloride regulation mediates local sleep pressure in the cortex. Nat. Neurosci. *26*, 64–78. 10.1038/s41593-022-01214-2.

47. Colonnese, M.T., and Phillips, M.A. (2018). Thalamocortical function in developing sensory circuits. Curr Opin Neurobiol *52*, 72–79. 10.1016/j.conb.2018.04.019.

48. Glanz, R., Sokoloff, G., and Blumberg, M.S. (2022). Neural decoding reveals specialized kinematic tuning after an abrupt cortical transition. Cell Rep *42*, 113119. 10.1016/j.celrep.2023.113119.

49. Glanz, R.M., Dooley, J.C., Sokoloff, G., and Blumberg, M.S. (2021). Sensory coding of limb kinematics in motor cortex across a key developmental transition. J Neurosci *41*, 6905–6918. 10.1523/jneurosci.0921-21.2021.

50. Butt, S.J., Stacey, J.A., Teramoto, Y., and Vagnoni, C. (2017). A role for GABAergic interneuron diversity in circuit development and plasticity of the neonatal cerebral cortex. Curr Opin Neurobiol *43*, 149–155. 10.1016/j.conb.2017.03.011.

51. Dard, R.F., Leprince, E., Denis, J., Balappa, S.R., Suchkov, D., Boyce, R., Lopez, C., Giorgi-Kurz, M., Szwagier, T., Dumont, T., et al. (2022). The rapid developmental rise of somatic inhibition disengages hippocampal dynamics from self-motion. Elife *11*. 10.7554/elife.78116.

52. Murata, Y., and Colonnese, M.T. (2019). Thalamic inhibitory circuits and network activity development. Brain Res *1706*, 13–23. 10.1016/j.brainres.2018.10.024.

53. Downes, N., and Mullins, P. (2014). The development of myelin in the brain of the juvenile rat. Toxicol Pathol *42*, 913–922. 10.1177/0192623313503518.

54. Grant, R.A., Mitchinson, B., and Prescott, T.J. (2012). The development of whisker control in rats in relation to locomotion. Dev Psychobiol *54*, 151–168.

55. Shriner, A.M., Drever, F.R., and Metz, G.A. (2009). The development of skilled walking in the rat. Behav Brain Res *205*, 10–10. 10.1016/j.bbr.2009.07.029.

56. Su, Y.-T., Gu, M.-Y., Chu, X., Feng, X., and Yu, Y.-Q. (2018). Whole-brain mapping of direct inputs to and axonal projections from GABAergic neurons in the parafacial zone. Neurosci Bull *34*, 485–496. 10.1007/s12264-018-0216-8.

57. Karlsson, K.Æ., Gall, A.J., Mohns, E.J., Seelke, A.M.H., and Blumberg, M.S. (2005). The neural substrates of infant sleep in rats. PLoS Biol *3*, e143. 10.1371/journal.pbio.0030143.

58. Todd, W.D., Gibson, J., Shaw, C., and Blumberg, M.S. (2010). Brainstem and hypothalamic regulation of sleep pressure and rebound in newborn rats. Behav Neurosci *124*, 69–78.

59. Clément, O., Sapin, E., Libourel, P.-A., Arthaud, S., Brischoux, F., Fort, P., and Luppi, P.-H. (2012). The lateral hypothalamic area controls paradoxical (REM) sleep by means of descending rojections to brainstem GABAergic neurons. J. Neurosci. *32*, 16763–16774. 10.1523/jneurosci.1885-12.2012.

60. Moore, J.D., Deschênes, M., Furuta, T., Huber, D., Smear, M.C., Demers, M., and Kleinfeld, D. (2013). Hierarchy of orofacial rhythms revealed through whisking and breathing. Nature *497*, 205–210. 10.1038/nature12076.

61. Kleinfeld, D., Deschênes, M., and Ulanovsky, N. (2016). Whisking, sniffing, and the hippocampal θ-rhythm: A tale of two oscillators. Plos Biol *14*, e1002385. 10.1371/journal.pbio.1002385.

62. Yang, C.F., and Feldman, J.L. (2018). Efferent projections of excitatory and inhibitory preBötzinger Complex neurons. J Comp Neurol *526*, 1389–1402. 10.1002/cne.24415.

63. Heck, D.H., Kozma, R., and Kay, L.M. (2019). The rhythm of memory: how breathing shapes memory function. J Neurophysiol *122*, 563–571. 10.1152/jn.00200.2019.

64. Jessberger, J., Zhong, W., Brankačk, J., and Draguhn, A. (2016). Olfactory bulb field potentials and respiration in sleep-wake states of mice. Neural Plast *2016*, 4570831. 10.1155/2016/4570831.

65. Mofleh, R., and Kocsis, B. (2021). Delta-range coupling between prefrontal cortex and hippocampus supported by respiratory rhythmic input from the olfactory bulb in freely behaving rats. Sci Rep *11*, 8100. 10.1038/s41598-021-87562-8.

66. Parnaudeau, S., Bolkan, S.S., and Kellendonk, C. (2017). The mediodorsal thalamus: An essential partner of the prefrontal cortex for cognition. Biol Psychiatry *83*, 648–656. 10.1016/j.biopsych.2017.11.008.

67. Lu, Y., Zhu, Z.-G., Ma, Q.-Q., Su, Y.-T., Han, Y., Wang, X., Duan, S., and Yu, Y.-Q. (2018). A critical time-window for the selective induction of hippocampal memory consolidation by a brief episode of slow-wave sleep. Neurosci. Bull. *34*, 1091–1099. 10.1007/s12264-018-0303-x.

68. Frank, M., Morrissette, R., and Heller, H. (1998). Effects of sleep deprivation in neonatal rats. Am J Physiol *44*, R148–R157.

69. Abbey, H., and Howard, E. (1973). Statistical procedure in developmental studies on species with multiple offspring. Dev Psychobiol *6*, 329–335.

70. Lazic, S.E., and Essioux, L. (2013). Improving basic and translational science by accounting for litter-to-litter variation in animal models. BMC Neurosci *14*, 37–37. 10.1186/1471-2202-14-37.

71. Gómez, L.J., Dooley, J.C., and Blumberg, M.S. (2023). Activity in developing prefrontal cortex is shaped by sleep and sensory experience. eLife *12*, e82103. 10.7554/elife.82103.

72. Dooley, J.C., and Blumberg, M.S. (2018). Developmental “awakening” of primary motor cortex to the sensory consequences of movement. eLife *7*, e41841. 10.7554/elife.41841.001.

73. Karlsson, K.Æ., Kreider, J., and Blumberg, M.S. (2004). Hypothalamic contribution to sleep-wake cycle development. Neuroscience *123*, 575–582.

74. Dooley, J.C., Glanz, R.M., Sokoloff, G., and Blumberg, M.S. (2020). Self-generated whisker movements drive state-dependent sensory Input to developing barrel cortex. Curr Biol *30*, 2404-2410.e4. 10.1016/j.cub.2020.04.045.

75. Dooley, J.C., Sokoloff, G., and Blumberg, M.S. (2021). Movements during sleep reveal the developmental emergence of a cerebellar-dependent internal model in motor thalamus. Curr Biol *31*, 5501–5511. 10.1016/j.cub.2021.10.014.

76. Gómez, L.J., Dooley, J.C., Sokoloff, G., and Blumberg, M.S. (2021). Parallel and serial sensory processing in developing primary somatosensory and motor cortex. J Neurosci *41*, 3418–3431. 10.1523/jneurosci.2614-20.2021.

77. Pachitariu, M., Steinmetz, N., Kadir, S., Carandini, M., and D., H.K. (2016). Kilosort: realtime spike-sorting for extracellular electrophysiology with hundreds of channels. Biorxiv, 061481. 10.1101/061481.

78. Rossant, C., and Harris, K.D. (2013). Hardware-accelerated interactive data visualization for neuroscience in Python. Front Neuroinform *7*, 36. 10.3389/fninf.2013.00036.

79. Mordkoff, J.T. (2019). A simple method for removing bias from a popular measure of standardized effect size: Adjusted partial eta squared. Adv. Methods Pr. Psychol. Sci. *2*, 228–232. 10.1177/2515245919855053.

80. Halverson, H.E., Kim, J., and Freeman, J.H. (2023). Dynamic changes in local activity and network interactions among the anterior cingulate, amygdala and cerebellum during associative learning. J. Neurosci. *43*, JN-RM-0731-23. 10.1523/jneurosci.0731-23.2023.

81. Nokia, M.S., Penttonen, M., Korhonen, T., and Wikgren, J. (2008). Hippocampal theta (3–8Hz) activity during classical eyeblink conditioning in rabbits. Neurobiology of Learning and Memory *90*, 62–70.

82. Wikgren, J., Nokia, M.S., and Penttonen, M. (2010). Hippocampo–cerebellar theta band phase synchrony in rabbits. Neuroscience *165*, 1538–1545.